Synthesis and Properties of Partially Fluorinated Aromatic Ionomers

A Doctoral Thesis
Presented to the
Integrated Graduate School of
Medicine, Engineering, and Agricultural Sciences

University of Yamanashi

March 2019

Jinju Ahn

Contents

Chapter 1. Introduction

1.1. Proton exchange membranes for application of PEMFC

Renewable energy sources like fuel cells have been promising to play a key role in the replacement of fossil fuels due to global energy concerns. Fuel cells efficiently convert chemical energy to electrical energy through an eco-friendly system. Fuel cells can be divided into five kinds according to the type of electrolyte: AFC (alkaline fuel cell), PEMFC (proton exchange membrane fuel cell), PAFC (phosphoric acid fuel cell), MCFC (molten carbonate fuel cell), and SOFC (solid oxide fuel cell). Among these, PEMFCs have been considered for application in transport and stationary and portable power generation. [1-5]

PEMFCs consist of anode, membrane, and cathode, as shown in Figure 1. The basic principle of a PEMFC is the reverse reaction of water electrolysis. At the anode, hydrogen gas generates electrons and protons. Protons are conducted from anode to cathode through the membrane; then, at the cathode, these protons, as well as the electrons, react with oxygen. The membrane is the fundamental component for PEMFC operation, because it supports ion transport from anode to cathode and prevents direct mixing of hydrogen and oxygen as a separator between the electrodes. The membranes are required to possess such qualities as high proton conductivity and high chemical and thermal stability.

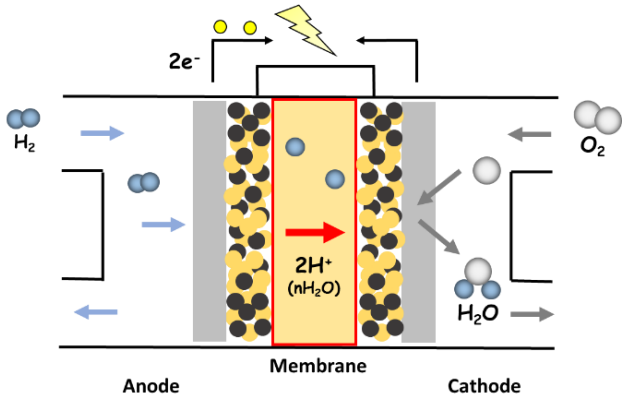

Anode : $H_2 \rightarrow 2H^+ + 2e^-$

Cathode : $½\ O_2 + 2H^+ + 2e^- \rightarrow H_2O$

Total: $H_2 + ½\ O_2 \rightarrow H_2O$

Figure 1. The structure of a polymer exchange membrane fuel cell

1.2. Perfluorosulfonic acid membranes and ionomers

The most famous and widely used commercial polymeric materials are the perfluorosulfonic acid ionomers Nafion, made by Dupont, and Flemion, made by Asahi Glass, as described in Figure 2. The perfluorosulfonic acid membrane is prepared by the radical copolymerization of tetrafluoroethylene (TFE) (the monomer in Teflon) and a derivative of a perfluoro (alkyl vinyl ether) with sulfonyl acid fluoride. The Teflon backbone of perfluorosulfonic acid ionomers contributes high chemical and mechanical stability and superior high proton conductivity due to the presence of superacid groups. However, the complications of the manufacturing process make it expensive, and the low thermal stability (< 100°C) leads to a limited narrow service temperature range. In addition, its high gas permeability results in low durability for long-term fuel cell performance. [6 - 9] For the commercialization of PEMFCs, alternative materials need to be developed and put forward for consideration.

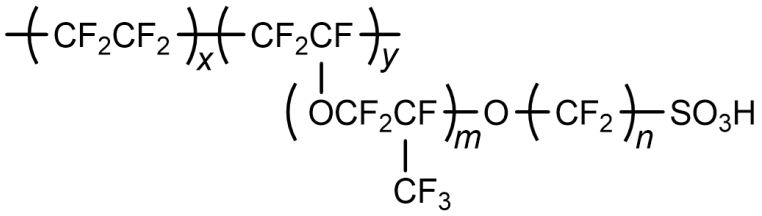

Nafion®, DuPont : m>1, n=2, x=5~13.5, y=1
Flemion®, AGC : m=0.1, n=1~5
Acipex®, Asahi Chemical : m=0.3, n=2~5, x=1.5~14

Figure 2. The chemical structure of perfluoro sulfonic acid ionomers

1.3. Sulfonated aromatic membranes

Many researchers have developed various alternative membranes to overcome the drawbacks of Nafion. The most attractive materials with the highest potential are sulfonated aromatic polymers, which are inexpensive, due to the simplicity of their synthetic process, and have high thermal stability and low gas permeability. There are several kinds of sulfonated aromatic polymers [10-19], the most prominent of which are SPEs (sulfonated poly (arylene ether)s); SPESs (sulfonated poly (ether sulfone)s) and SPEEKs (sulfonated poly (ether ether ketone)s), SPPs (sulfonated poly (p-phenylene)s), and SPIs (sulfonated polyimides).

Among these, SPE membranes like SPES and SPEEK have extensively been researched, as shown

in Figure 3. These materials have been prepared by direct polymerization between the OH-terminated and halide-terminated (F and Cl) monomers. Many research groups have reported effective structures and investigated their membrane properties. The SPEs membranes can be prepared as structurally random or as block polymers with high molecular weight and high proton conductivity. However, when compared with the Nafion membrane, they still have significantly lower proton conductivity under low humidity conditions (< 50 % RH), even though it has higher water uptake due to higher ion exchange capacity (IEC). Moreover, the SPE membranes have insufficient performance during cell operation, due to lower oxidative and mechanical stability.

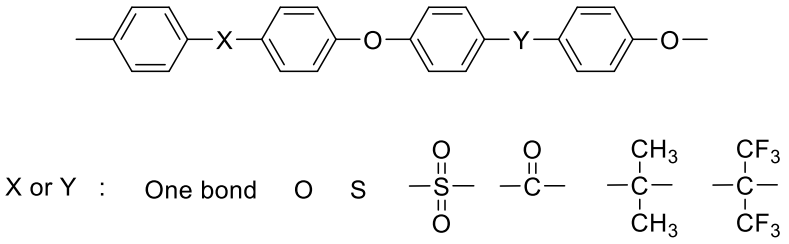

Figure 3. Chemical structures of aromatic materials

The SPP (sulfonated poly(p-phenylene)s) membranes have been considered to be important due to expected higher oxidative stability. As opposed to SPE membranes, SPPs consist of benzene rings without heteroatom groups (ether, sulfone, ketone, and so on) which are chemically vulnerable under fuel cell operation conditions. In general, the SPP membranes are very stiff, with insufficient elongation, due to the rigid polymer backbone, containing para-linked benzene rings. Generally, the poly(p-phenylene)s are highly crystalline, rigid rod polymers that are difficult to handle due to their very low flexibility and low solubility in organic solvents, which impose limits on the formation of membranes for applications and property testing. Several researchers have suggested ways to overcome these kinds of drawbacks through the use of modified poly(p-phenylene)s.

McGrath and coworkers reported soluble sulfonated poly(p-phenylene) derivatives [20], which were prepared by Ni-catalyzed coupling polymerization with aryl-substituted 2,5-dichlorobenzophenone, as shown in Figure 4. Even though it is possible to prepare homo- and co-polymer membranes, the obtained membranes are very brittle. However, non-sulfonated polymers showed high thermal stability, with only 5% weight loss at temperatures over 480°C. This polymer was blended or composited with fiberglass fabric and PEPO (poly(arylene ether phenyl phosphine oxide)). The proton conductivity of those polymers exhibited 90-110 mS cm^{-1}, measured on a polymer composite made from fiberglass fabric and resin (40/60 w/w).

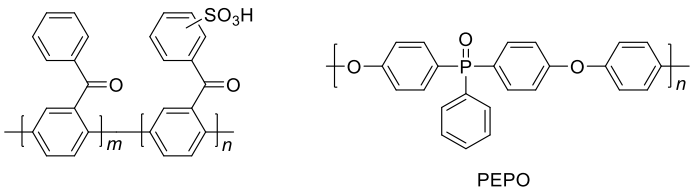

Figure 4. Chemical structures of sulfonated poly(p-phenylene) derivatives with 2,5-dichlorobenzophenone and PEPO

Holdcroft and coworkers designed and prepared phenylated polyphenylene ionomers [21, 22] by Diel-Alder polymerization reaction, as shown in Figure 5. Sulfophenylated polyphenylenes are obtained by incorporation of spacer units, biphenyl (sPPP-H^+) and naphthyl (sPPN-H^+), in the polymer backbone. The sPPP-H^+ and sPPN-H^+ membranes have excellent tensile strength, Young's modulus (59.6 MPa for sPPB-H^+ and 1331Mpa for sPPN-H^+, respectively). As expected, they had low elongation at break (17.5%) under dry conditions. Furthermore, the high durability of the membrane was confirmed under accelerated stress testing, maintaining high conductivity even after 400 hours due to its high oxidative stability.

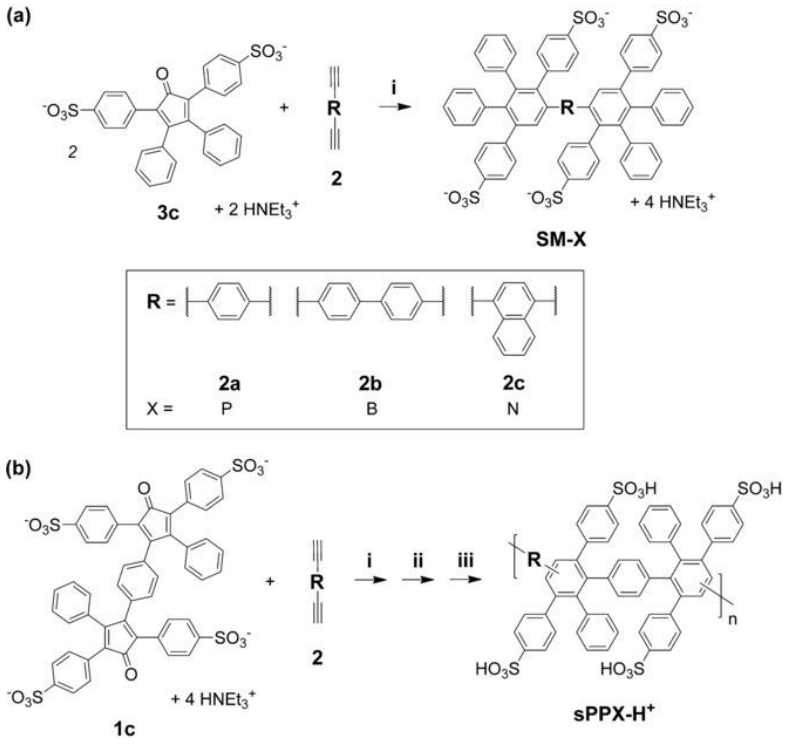

Figure 5. Chemical structures of sulfophenylated polyphenylenes adapted from [22].

In our laboratory, we developed and synthesized a simpler version of sulfonated polyphenylene (SPP-QP) [23] composed only of phenylene rings and sulfonic acid groups, as described in Figure 6. Although the SPP-QP membranes consisted of only benzene rings, m- and p-phenylene and sulfonated monomer, by carefully optimizing the m-/p- composition and ion exchange capacity (IEC), we proved that sulfonated polyphenylene with a very simple polymer structure provided flexible and bendable thin membranes with high proton conductivity and superior oxidative stability in comparison with SPK membranes.

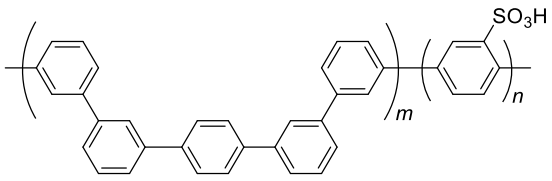

Figure 6. Chemical structures of sulfonated poly(phenylene) (SPP-QP) composed only of phenylene rings and sulfonic acid groups. [23]

Recently developed sulfonated aromatic materials have been researched and have achieved much higher performance than before. However, we still need to overcome several deficiencies of the membrane properties like proton conductivity, particularly under low humidity conditions, oxidative stability, mechanical stability with reasonable hydrated dimensional stability and compatibility with catalyst layers.

1.3.1. Proton transport mechanism

The major function of the membrane is proton conductivity. According to the literature, ion transport [24-26] in the membrane is generally explained by three mechanisms, Grotthus (hopping), vehicular (diffusion) and surface-mediated transport, as described in Figure 7. The vehicular mechanism is the movement of larger cations like water-solvated species ($H_2O_2^+$, $H_9O_4^+$, etc.). In contrast to other cations, protons may also move via structural diffusion which is referred to as the Grotthus mechanism. The bound nature of the counter anion (-SO_3- in the case of sulfonic acid-base polymer electrolytes) also presents a third mode for proton transport, surface transport. In this mechanism, protons are believed to be transported between -SO_3- groups located on the walls of hydrophilic channels, but this model of transport has a high activation energy. In systems with relatively high water contents, it is

likely that vehicular and Grotthus mechanisms predominate.

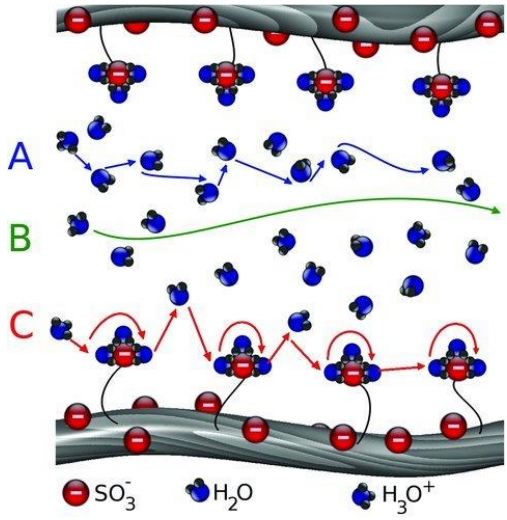

Figure 7. Schematic illustration of different modes of proton conduction in a solid polymer electrolyte where A = Grotthus, B = vehicular, and C = surface mechanisms. Adapted from [26].

As a conclusion based on the literature, we can understand that proton conductivity is strongly related to water utilization in the hydrophilic part of the polymer containing -SO_3H- groups. According to that, not only higher ion exchange capacity (IEC) of the membrane but also a higher concentration of sulfonic acid groups (-SO_3H) lead to both higher water uptake and higher proton conductivity. Even though high water uptake supports high proton conductivity, it also could cause excess swelling of the membrane, leading to dimensional instability. Furthermore, excess swelling of membranes usually can cause fatally low durability in wet-dry cycling during fuel cell operation. Therefore, we need to find optimized membranes offering a balance between water uptake and proton conductivity and prove that the membranes are sufficiently optimized by evaluation of the proton conductivity and mechanical stability under a range of humidity conditions.

1.3.2. The design for property improvement

To improve the proton conductivity, three main approaches can be considered for the synthesis: 1) control of ion exchange capacity (IEC); 2) introduction of high acidity and high concentration of sulfonic acid groups; and 3) promotion of structural block polymers for well-developed phase separation between hydrophilic and hydrophobic parts.

1.3.3. Control of IEC of polymer

To control ion exchange capacity (IEC) by synthetic methods would be an easy, simple way to improve proton conductivity. There are two ways to prepare sulfonated aromatic polymers: direct polymerization with pre-sulfonated monomers and post-sulfonation after polymerization. In general, the direct polymerization with pre-sulfonated monomers is convenient to control the IEC of a polymer by controlling the feed ratio of pre-sulfonated monomers. However, lower molecular weight of the obtained polymers occurs due to relatively lower reactivity of the sulfonated monomer. On the other hand, post-sulfonation after polymerization could provide higher molecular weight of polymers with higher reactivity of the monomers in comparison with pre-sulfonated monomers. However, the inefficient post-sulfonation reaction of polymers, with low yield (less than 60%), makes it difficult to control IEC, and the need for a second step to produce the targeted sulfonated polymer is not attractive for commercialization. Even though high water uptake supports high proton conductivity, it also could cause excess swelling of the membrane, leading to dimensional instability with the Nafion ionomer in the catalyst layer. If the IEC value of a membrane is excessively high, it could result either in significant swelling of the membrane dimensions or its dissolution in water, depending on its properties.[26, 27]

1.3.3.1. Control of acidity and concentration of sulfonic acid groups

The second approach, to control the acidity of the sulfonic acid group, for example, using a higher acidity group like a fluoroalkyl sulfonic acid or introducing a high concentration of sulfonic acid groups on the polymeric material, can be considered. According to this general approach, many researchers have suggested specific approaches, as follows.

Chulsung Bae and coworkers [28, 29] reported the effects of the acidity of sulfonic acid groups on membrane properties, especially on proton conductivity and morphology, as described in Figure 8. Three types of SEBS ionomers with different strength acidic groups, like fluoro alkylsulfonic acid, arylsulfonic acid and arylphosphonic acid, were prepared by the palladium-catalyzed Suzuki-Miyaura

cross reaction. The higher acidity groups like the fluoroalkyl sulfonic acid exhibited significantly higher proton conductivity than the less acidic aryl and alkyl sulfonated ionomers with higher water uptake. As expected, higher acidity of the sulfonic acid led to higher proton conductivity, although all polymers needed to be prepared by the post-sulfonation method.

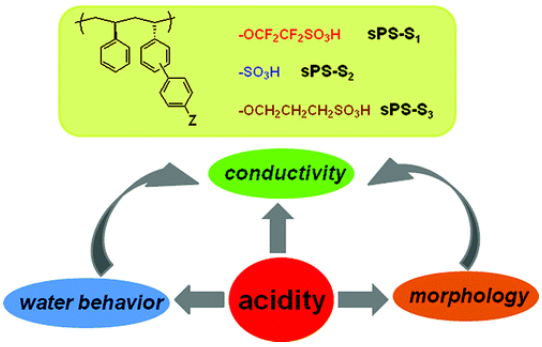

Figure 8. The chemical structure of SEBS ionomers with different strength acidic groups like fluoroalkylsulfonic acid, arylsulfonic acid and arylphosphonic acid with expected effects [28].

Byungchan Bae and coworkers [30, 31] reported a high concentration of sulfonic acid groups as the hydrophilic part of multi-block SPES membranes, as shown in Figure 9. The SPES polymers obtained with higher concentrations of sulfonic acid groups have higher water uptake and higher proton conductivity, due to their well-developed phase separation between hydrophilic and hydrophobic parts in TEM images with similar IEC.

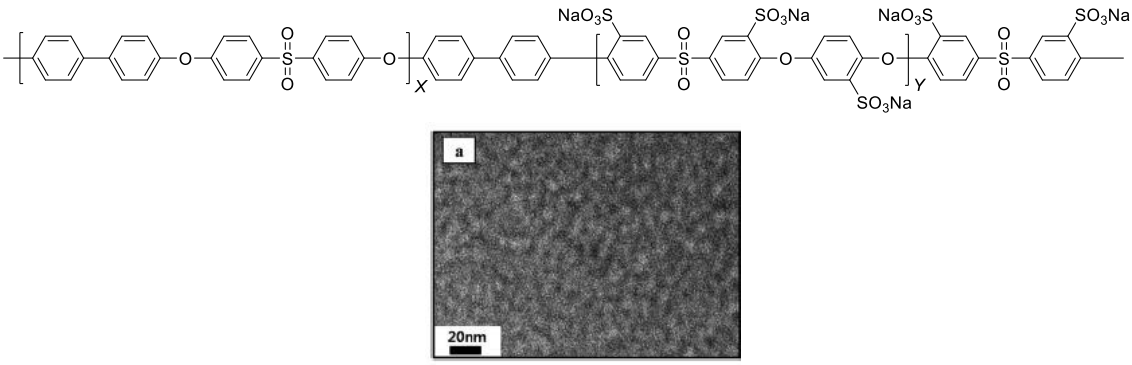

Figure 9. The chemical structure and TEM image of Block SPAES (IEC 2.8 mequiv g^{-1}); high concentration of sulfonic acid group on hydrophilic part of multi-block SPES polymers [31]

Ueda and coworkers [32] reported locally and densely sulfonated poly(ether sulfone)s membranes, as shown in Figure 10. The polymers were synthesized by nucleophilic substitution 4, 4' - dichlorodiphenyl sulfone with 1, 2, 4, 5 - tetrakis ([1, 1' - biphenyl] - 2 - oxy) - 3, 6 - bis (4 -

hydrozyphenoxy) benzene and 2,2'- bis (4 -hydroxyphenyl) hexafluoropropane, followed by sulfonation using chlorosulfonic acid. The large difference in polarity between the locally and densely sulfonated units and hydrophobic units of the polymers resulted in the formation of well-defined phase-separated structures, which enabled efficient proton conduction over a wide relative humidity range (30 - 95 %RH) at 80 °C.

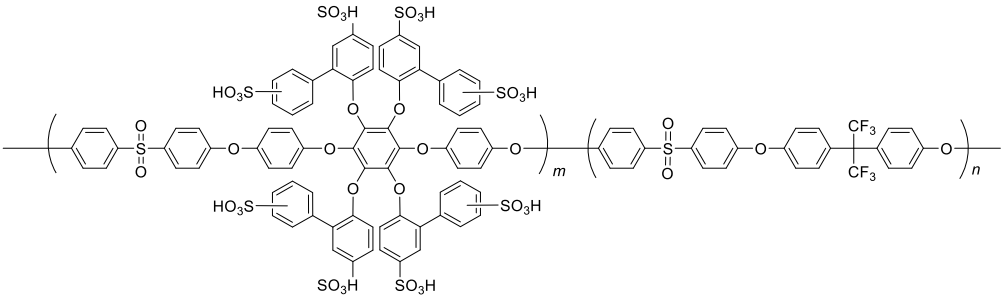

Figure 10. The chemical structure of locally and densely sulfonated poly(ether sulfone)s membrane [32].

As a result, we could expect high acidity and locally and densely concentrated sulfonic acid groups in the membrane could be a helpful and effective approach to improve proton conductivity because of improved water uptake and the influence of well-developed phase separation between hydrophilic and hydrophobic moieties.

1.3.3.2. Well-developed phase separation between hydrophilic and hydrophobic parts as block-polymers

Previously, sulfonated polymers like SPEs membranes were mainly developed as statistically random polymers. To improve proton conductivity, the chemical structure of the polymer was artificially made to produce multi-block polymers to boost the formation of wider water pathways to transport protons more effectively, similar to having a locally highly dense concentration of sulfonic acid groups on the hydrophilic part and also introducing a strongly hydrophobic part. According to this approach, many researchers have suggested specific approaches, as follows.

Na and coworkers [33] reported block sulfonated poly(ether ether ketone)s (SPEEKs) materials, prepared and characterized as described in Figure 11. The block and random SPEEK membranes were prepared and compared. Both membranes were obtained with high molecular weight and offered tough membranes. The block SPEEK membrane had higher proton conductivity (0.03 S cm^{-1}), even though it had lower IEC (0.488 mequiv g^{-1}) than those of a random SPEEK membrane (0.02 S cm^{-1}) at 80°C.

This result is related to the larger ionic cluster size in SAXS profiles. This must be due to the influence of larger ionic cluster size on improved proton conductivity.

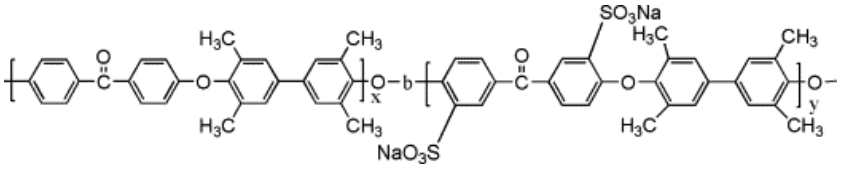

Figure 11. The chemical structure of block sulfonated SPEEKs [33].

Recently, our laboratory has considered that a block (statistical) chemical structure could cause higher proton conductivity due to its larger hydrophilic cluster size of phase separation that has an influence on well-connected water pathways; however, it also could make it inhomogeneous on the surface of the membrane, as described in Figure 12. According to a reference [34], both cells, the multiblock-cell and random-cell, have similar proton conductivities, but the multiblock-cell possessed lower mass activity than the random-cell, i.e., lower cell performance. Rather, this indicates that the well-developed phase separation of the block polymer is not compatible with the catalyst layer, resulting in low performance. Additionally, it could be favorable for the transport of protons with high water content in the membrane, but for the catalyst layer, a high degree of water swelling has adverse effects, like blocking the pores of the catalyst or gas diffusion layers, limiting reactant mass transport. The excessive water swelling in the membrane and ionomer might favor the lower mass activity of the catalyst. In general, sulfonated aromatic membranes have higher water uptake than the Nafion ionomer in the catalyst layer. There could also be dimensional and interfacial resistance during cell operation. That is why we need to find high proton conductivity of the membrane with a low water swelling ratio. [26, 27, 34].

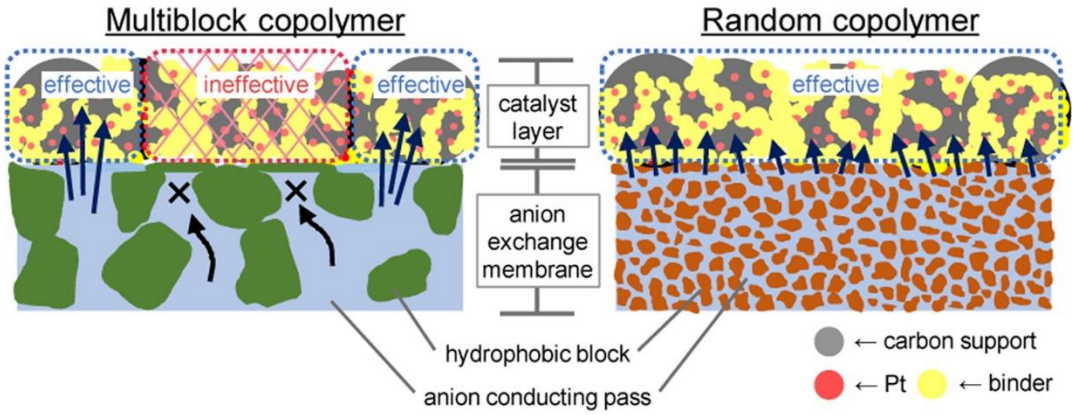

Figure 12. The expected pathway to conduct ions on the surface of the anion exchange membrane, dependent on the multi-block and random copolymer [34].

1.4. The objective of the research

As explained above, many researchers have been contributing to the development of replacements for perfluorosulfonic acid membranes. The sulfonated aromatic polymers, as the most promising alternative materials, are very attractive due to their high thermal ability and low gas permeability. However, novel and effective polymeric materials are necessary to improve several properties, such as proton conductivity, chemical stability, mechanical stability and compatibility with the catalyst layer with PFSA ionomers, for good cell performance. To suggest ways to improve these properties, I have sought to find out which structures could be effective and helpful.

In Chapter 2, sulfonated terpolymers containing perfluoroalkylene and alkylene groups on the backbone of poly(phenylene) (SPA terpolymers) were obtained. By introducing perfluoroalkylene and alkylene groups, I could expect to improve the solubility and flexibility of poly(phenylene)s, and I determined the effects of chemical structure on membrane properties such as proton conductivity, water uptake, mechanical stability and cell performance [35].

In Chapter 3, sulfonated aromatic polymers (SBAF) containing hexafluoroisopropylidene (CF_3-CF_3) groups were suggested and investigated in the same way as in Chapter 2. The effects of hexafluoroisopropylidene (CF_3-CF_3) groups were determined by comparing with previously developed sulfonated poly(phenylene)s (SPP - QP) membranes. The expected benefits of hexafluoroisopropylidene (CF_3-CF_3) groups on the main chain would be flexibility and solubility [36].

In Chapter 4, novel partially fluorinated polymers (STF) were suggested and designed to investigate the effects of the trifluoromethyl group. For polymerization, various types of STF polymers were considered, like different combinations of para-, ortho- and meta-types of dichloro-benzo or -biphenyl trifluoride monomers. In comparison with SBAF polymers, STF polymer properties were determined.

References

[1] L. Carrette, K. A. Friedrich, U. Stimming, *Fuel Cells*, 2001, 1, 5-39.

[2] O. Z. Sharaf, M. F. Orhan, *Renew. Sustain. Energy Rev.*, 2014, 32,.810-853.

[3] T. Wilberforce, A. Alaswad, A. Palumbo, M. Dassisti and A. G. Olabi, *Int. J. Hydrogen Energy*, 2016, 41, 16509-16522.

[4] U. Lucia, *Renewable and Sustain. Energy Rev.*, 2014, 30, 164-169.

[5] Y. Wang, K. S. Chen, J. Mishler, S. C. Cho and X. C. Adroher, *Appl. Energy*, 2011, 88, 981-1007.

[6] K. A. Mauritz, R. B. Moore, *Chem. Rev.*, 2004, 104, 4535-4586.

[7] D. E. Curtin, R. D. Lousenberg, T. J. Henry, P. C. Tangeman, and M. E. Tisack, *J. Power Sources*, 2004, 131, 41-48.

[8] K. Broka and P. Ekdunge, *J. Appl. Electrochem.*, 1997, 27, 117-123.

[9] Y. Tang, A. M. Karlsson, M. H. Santare, M. Gilbert and Johnson, W. B., *Mater. Sci. Eng.*, 2006, 425, 297-304.

[10] M. A. Hickner and B. S. Pivovar, *Fuel Cells*, 2005, 5, 213-228

[11] K. Goto, I. Rozhanskii and Y. Yamakawa, *Polym. J.*, 2009, 41, 95-104

[12] A. Ghosh and S. Banerjee, *e-polymer*, 2014, 14, 227-257

[13] C. H. Park, C. H. Lee, M. D. Guiver and Y. M. Lee, *J. Prog. Polym. Sci.*, 2011, 36, 1443-1498

[14] M. A. Hickner, H. Ghassemi, Y. S. Kim, B. R. Einsla and J. E. McGrath, *Chem. Rev.*, 2004, 104, 4587-4612

[15] W. L. Harrison, M. A. Hickner, Y. S. Kim and J. E. McGrath, *Fuel Cells*, 2005, 5, 201-212

[16] J. Miyake and K. Miyatake, *Polym. J.*, 2017, 49, 487-495.

[17] S. Takamuku, A. Wohlfarth, A. Manhart and P. Rader, P. Jannasch, *Polym. Chem*., 2015, 6, 1267-1274.

[18] B. Wang, Z. Cai, N. Zhang, B. Zhang, D. Qi, C. Zhao and H. Na, *RSC Adv.*, 2015, 5, 536-544.

[19] A. Singh, S. Banerjee, H. Komber and B. Voit, *RSC Adv.*, 2016, 6, 13478-13489.

[20] H. Ghassemi and J. E. McGrath, *Polymer*, 2004, 5847-5854

[21] T. J. G. Skalaski, B. Britton, T. J. Peckham and S. Holdcroft, *J. Am. Chem. Soc.*, 2015, 137, 12223-12226.

[22] M. Adamski, T. J. G. Skalaski, B. Britton, T. J. Peckham, L. Metzler and S. Holdcroft, *Angew. Chem. Int. Ed.*, 2017, 56, 9058-9061.

[23] J. Miyake, R. Taki, T. Mochizuki, R. Shimizu, R. Akiyama, M. Uchida and K. Miyatake, *Sci.*

Adv., 2017, 3, eaao0476.

[24] H. Hou, M. L. DiVona, P. Knauth, *ChemSuschem*, 2011, 4, 1526-1536

[25] K. D. Kreuer, A. Rabenau, W. Weppner, *Angew. Chem.-Int. Ed.*, 1982, 21, 208-209

[26] T. J. Peckham and S. Holdcroft, *Adv. Mater.*, 2010, 22, 4667-4690

[27] W. Dai, H. Wang, X. Yuan, J. J. Martin, D. Yang, J. Qiao and J. Ma, *Int. J. Hydrogen Energy*, 2009, 34, 9461-9478

[28] Y. Chang, G. F. Brunello, J. Fuller, M. Hawley, Y. S. Kim, M. Disabb-Miller, M. A. Hickner, S. S. Jang and C. Bae, *Macromolecules*, 2011, 44, 8485-8469

[29] B. Date, J. Han, S. Park, D. Shin, C. Y. Ryu and C. Bae, *Macromolecules*, 2018, 51, 1020-1030

[30] J. Ahn, H. Lee, T. Yang, C. Kim and B. Bae, *J. Polym. Sci. Part A: Polym. Chem.*, 2014, 52, 2947-2957

[31] S. Lee, J. Ahn, H. Lee, J. Kim, C. Kim, T. Yang and B. Bae, *J. Mater. Chem. A.*, 2015, 3, 1833-1836

[32] K. Matsumoto, T. Higashihara and M. Ueda, *Macromolecules*, 2009, 42, 1161-1166

[33] C. Zhao, H. Lin, K. Shao, X. Li, H. Ni, Z. Wang and H. Na, *J. Power. Sources*, 2006, 162, 1003-1009

[34] M. Hara, T. Kimura, T. Nakamura, M. Shimada, H. Ono, S. Shimada, K. Miyatake, M. Uchida, J. Inukai and M. Watanabe, *Langmiur*, 2016, 32, 9557-9565

[35] J. Ahn, K. Miyatake, *ACS Appl Energy Mater.*, 2018, DOI:10.1021/acsaem.8b00684

[36] J. Ahn, R. Simizu, K. Miyatake, *J. Mater. Chem. A.*, 2018, DOI: 10.1039/c8ta09587f

Chapter 2. Sulfonated terpolymers containing alkylene and perfluoroalkylene groups: effect of aliphatic groups on membrane properties

2.1. Introduction

In Chapter 1, as explained, sulfonated aromatic materials [1 - 4] have probably been the most investigated because of their large freedom in molecular design, including main chain and side chain structures, sequences of copolymer components, positions and number of acidic groups, etc. [5 - 7] Recently, we have successfully developed sulfonated polyphenylenes composed solely of sulfonic acid groups and phenylene rings.[8] The polyphenylene ionomer membranes exhibited high proton conductivity and chemical stability, leading to high fuel cell performance and durability. Unlike typical sulfonated aromatic (co)polymers, lack of heteroatom linkages, such as ether, sulfide, and sulfone groups in the polyphenylene ionomer main chain, was effective in achieving high oxidative stability of the membranes.

In addition to the bulk properties, interfacial compatibility with the catalyst layers is highly crucial for PEMs in practically operating fuel cells. Since PFSA ionomers are generally used as proton conducting binders in the catalyst layers, incompatibility of the perfluorinated and nonfluorinated ionomer materials often impedes transport of protons and water at the interface of the catalyst layers and PEMs. In order to mitigate the interfacial issues, we have proposed a partially fluorinated sulfonated polyphenylene (SPAF, Figure 13) membrane [9]. Because of its well-defined molecular structure with small-scale phase-separated morphology, similar to those of the PFSA membranes, the SPAF membrane had an improved interfacial contact with the catalyst layers and exhibited high cathode performance. The proton conductivity of the SPAF membrane, however, still needed to be improved at low humidity.

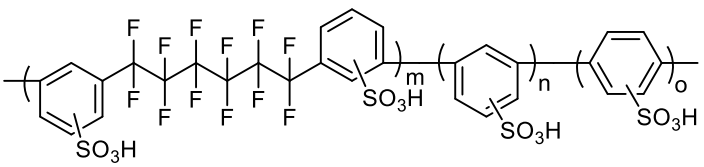

Figure 13. The structure of partially fluorinated sulfonated polyphenylene (SPAF)

The objective of the present research is to synthesize a series of terpolymers (SPA) composed of sulfophenylene, perfluoroalkylene, and alkylene groups, and to evaluate the effect of the aliphatic components in the main chain on the bulk and interfacial properties of the resulting PEMs. Three types of SPA membranes, SPA-A, -B and –C with different ion exchange capacities (IECs), were prepared by changing the terpolymer compositions. In the SPA-C case, we modified the SPAF terpolymer to obtain a higher IEC membrane. In previous research on SPAF, it was prepared by a post-sulfonation process; in this research, I selected direct polymerization with sulfonated monomers due to its easy and economical manufacturing process. The properties of the SPA membranes, including proton conductivity, water absorbability, mechanical properties, and fuel cell performance and durability, have been studied and compared with those of the SPAF membrane.

2.2. Measurements

^{1}H and ^{19}F NMR spectra were measured with a JEOL JNM-ECA/ECX500 using deuterated chloroform ($CDCl_3$) or dimethyl sulfoxide (DMSO-d_6) with tetramethylsilane as an internal reference. The molecular weight was measured via gel permeation chromatography (GPC) equipped with a Jasco 805 UV detector. Dimethylformamide (DMF) containing 0.01 M lithium bromide (LiBr) was used as eluent. Shodex KF-805L column was used for the measurement of polymers and monomers. Molecular weight was calibrated using standard polystyrene samples.

Ion exchange capacity (IEC) of the membranes was measured by titration at r.t. A piece of dry membrane in acid form was immersed into 2 M NaCl aqueous solution for at least 24 h. The solution was titrated with 0.1 M NaOH aqueous solution. The IEC was calculated using the following equation; IEC (mequiv. g^{-1}) = $\Delta V_{NaOH} \times C_{NaOH} / W_d$, where W_d is weight of dry membrane, ΔV_{NaOH} is consumed volume of the NaOH solution, and C_{NaOH} is the concentration of the NaOH solution.

Morphology of the membranes was analyzed by transmission electron microscopy (TEM). For TEM observation, the membranes were stained with lead ions (Pb^{2+}) by ion exchange of the sulfonic acid groups in 0.5 M $Pb(OAc)_2$ aqueous solution, rinsed with deionized water, and dried in a vacuum oven for 12 h. The stained samples were embedded in epoxy resin, sectioned into 50 nm slices with a Leica microtome Ultracut UCT, placed on copper grids, and then investigated with a Hitachi H-9500 TEM at an acceleration voltage of 200 kV.

The proton conductivity and water uptake were measured with a solid electrolyte analyzer system

(MSBAD-V-FC, Bel Japan Co.) equipped with a temperature and humidity controllable chamber. The weight of the membranes at a given humidity was measured by magnetic suspension balance. The water uptake was calculated by the following equation. Water uptake = (weight of hydrated membrane) – (weight of dry membrane) / weight of dry membrane × 100. The membranes were dried at 80 ºC for 3 h under vacuum to obtain the weight of dry membranes and exposed to the set humidity for at least 2 h to obtain the weight of hydrated membranes. In-plane proton conductivity (σ) of the membranes was measured by ac impedance spectroscopy (Solartron 1255B and 1287) simultaneously in the same chamber. Ion conducting resistances (R) were determined from the impedance plot measured over the frequency range from 1 to 10^5 Hz. The proton conductivity was calculated according to the following equation; $\sigma = L / (S \times R)$, where L and S are the distance of the electrodes and the cross-sectional area of the membrane, respectively.

Dynamic mechanical analyses (DMA) of the membranes (5 mm × 30 mm) were carried out by an ITK DVA-225 dynamic viscoelastic analyzer at 80 ºC from 0 to 90% RH at 10 Hz. The storage moduli (E'), loss moduli (E''), and tan σ (= E''/E') of the membranes were measured. Tensile strength of the membranes was measured with a Shimadzu AGS-J 500N universal test machine attached with a Toshin Kogyo Bethel-3A temperature and humidity controllable chamber at 80 ºC and 60% RH at a stretching rate of 10 mm min^{-1}. Stress versus strain curves were obtained for samples cut into a dumbbell shape (DIN-53503-S3, 35 mm × 6 mm (total) and 12 mm × 2 mm (test area)).

A catalyst paste was prepared by mixing Pt/CB catalyst (TEC10E50E, Tanaka Kikinzoku Kogyo K. K.), Nafion dispersion (IEC = 0.95-1.03 mequiv g^{-1}, D-521, Du Pont), deionized water and ethanol by ball milling for 30 min. The mass ratio of Nafion ionomer to the carbon support (I/C) was adjusted to 0.7. The catalyst-coated membranes (CCMs) were prepared by spraying the catalyst paste on both sides of SPA-B membranes (IEC = 2.51 mequiv g^{-1}, 29 μm thick) by pulse swirl spray (PSS) technique. The CCMs were dried at 60 ºC overnight and hot-pressed at 140 ºC and 1.0 MPa for 3 min. The geometric area and the Pt loading amount of the catalyst layer (CL) were 4.41 cm^2 and 0.5 mg cm^{-2}, respectively. The CCMs were sandwiched by two gas diffusion layers and mounted into a cell which had serpentine flow channels on both the anode and the cathode sides.

Linear sweep voltammetry (LSV) was measured to evaluate the permeability of hydrogen gas from the anode to the cathode through the membrane. LSV measurement was carried out at 80 ºC and 100% RH. Prior to the LSV measurements, hydrogen (100 mL min^{-1}) and nitrogen (100 mL min^{-1}) were supplied to the anode and the cathode, respectively. The cathode potential was swept from 0.15 to 0.60

V at a scan rate of 0.5 mV s^{-1}. To evaluate the cell performance, the polarization curves were measured at 80 ºC, 30% and 100% RH. Pure hydrogen for the anode and air or oxygen for the cathode were supplied. The gas utilizations at the anode and the cathode were 70% and 40%, respectively. The open circuit voltage (OCV) hold test was carried out at 80 ºC and 30% RH. Pure hydrogen and air at a gas flow rate of 100 mL min^{-1} were supplied to the anode and the cathode, respectively. The OCV hold test was continued for 1000 h.

2.3. Experimental

2.3.1. Materials

1-Chloro-3-iodobenzene (> 97%, TCI), copper (Cu) powder (particle size 75-150 μm, > 99%, Kanto Chemical), dimethyl sulfoxide (DMSO) (> 99%, Kanto Chemical), chlorobenzene (98%, TCI), aluminum (III) chloride (> 98%, TCI), adipoyl chloride (98%, TCI), 2-propanol, sebacoyl chloride (> 95%, TCI), triethylsilane (ET_3SiH) (> 98%, TCI), trifluoroacetic acid (TFA) (> 99%, TCI), 2,5-dichlorobenzenesulfonic acid dehydrate (SP) (TCI), bis(1,5-cyclooctadiene)nickel(0) ($Ni(COD)_2$) (> 95%, Kanto Chemical), 2,2'-bipyridine (> 99%, Kanto Chemical), potassium carbonate (K_2CO_3) (Kanto Chemical), sodium chloride (NaCl) (Kanto Chemical) were used as received. 1, 6-Diiodoperfluorohexane was kindly supplied by Tosoh Finechem Co. Monomers 1 containing perfluoroalkylene groups was synthesized by Maloughlin-Thrower reaction and 2 containing alkylene groups were synthesized according to the literature [10, 11].

2.3.2. Polymerization of terpolymer (SPA-A and B)

A typical procedure for SPA-A is as follows. A 100 mL three-neck flask was charged with monomer (1) (0.2616 g, 0.5 mmol), monomer (2) (0.2378 g, 0.5 mmol), SP (0.4930 g, 1.76 mmol), K_2CO_3 (0.2919 g, 2.112 mmol), 2,2'-bipyridine (0.9053 g, 5.796 mmol), dimethyl sulfoxide (DMSO, 6 mL), and toluene (6 mL). The mixture was heated at 170 ºC for 2 h with a Dean Stark trap under N_2. After azeotropic dehydration, the mixture was cooled to 80 ºC. To the mixture, $Ni(COD)_2$ (1.6000g, 5.796 mmol) was added. After the reaction at 80 ºC for 3 h, the mixture was poured into a large excess of 6 M HCl to precipitate the product. The crude product was washed with concentrated HCl and deionized water several times. The targeted terpolymer was obtained by drying at 80 ºC in a vacuum oven overnight in 89 - 95% yield.

2.3.3. Membrane preparation and Acidification

A terpolymer in sodium ion form was dissolved in DMSO (5 - 10% w/v). The solution was cast onto a clean glass plate and dried at 80 ºC for 1 d. The resulting membranes (ca. 60 μm thick) were converted to acid form with 1 M H_2SO_4 for 1 d at room temperature, washed with deionized water several times, and dried at r.t.

2.4. Results and discussion

2.4.1. Synthesis of Terpolymers (SPA)

A series of novel terpolymers (SPA) composed of sulfonated phenylene, alkylene, and perfluoroalkylene groups was synthesized via Ni(0)-promoted coupling reaction (Scheme 1). The feed ratio of the monomer 1 containing perfluoroalkylene group and the monomer 2 containing alkylene group was controlled so as to evaluate its effect on the membrane properties. The feed ratio of 2,5-dichlorobenzenesulfonic acid (SP) monomer to the aliphatic monomers (1 and 2) was adjusted to obtain SPA terpolymers with targeted IEC ranging from 1.7 to 3.4 mequiv g^{-1}. The terpolymerization reaction proceeded well in DMSO solution to provide the corresponding products in high yields (~ 94%). The resulting terpolymers were soluble in polar organic solvents such as DMAc, DMSO, and NMP. The chemical structure of the terpolymers was analyzed by ^{1}H and ^{19}F NMR spectra (Figure 14). In the ^{1}H NMR spectra, aromatic and aliphatic protons were assigned to the supposed structure although the composition of the components could not be determined due to the significant overlapping of the aromatic peaks. In the ^{19}F NMR spectra, three characteristic peaks for perfluorohexylene groups were observed at slightly lower magnetic fields than those of the monomer 1. The results indicate successful formation of the targeted SPA terpolymers. The molecular weight of the SPA-A and -B terpolymers was estimated by GPC to be Mn = 61 - 104 kDa and Mw = 134 - 183 kDa, respectively (Table 1 and Figure 15). SPA-C polymers were obtained in lower molecular weight, indicating lower reactivity of the monomer 1 than 2. The dispersity (PDI) was 1.7 - 2.2 and reasonable for this type of polycondensation reaction. The apparent molecular weight was higher with increasing the SP content presumably because of the larger radius of gyration of the terpolymers with higher IEC values (or higher content of the sulfonic acid groups).

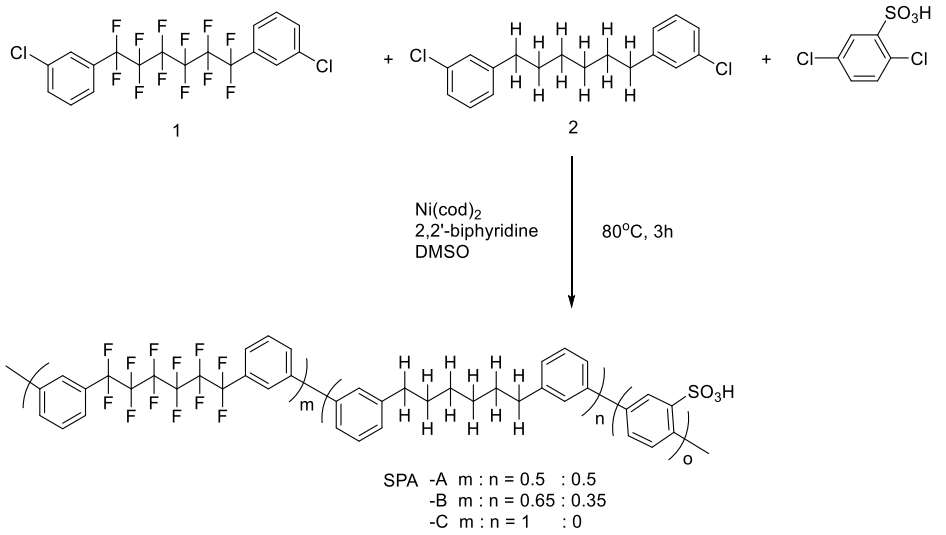

Scheme 1. Synthesis of SPA terpolymers composed of perfluoroalkylene, alkylene, and sulfonated phenylene groups.

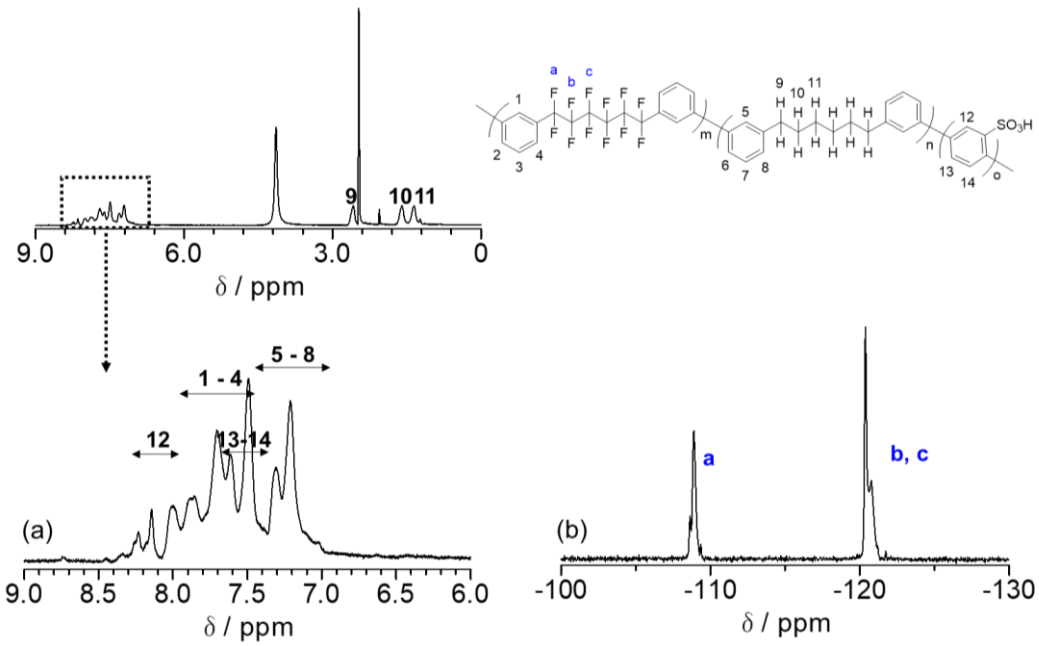

Figure 14. (a) ^{1}H and (b)^{19}F NMR spectra of SPA terpolymer in DMSO-d_6 at 80 ºC.

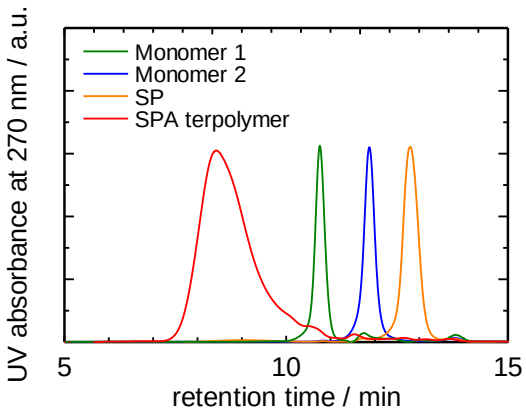

Figure 15. GPC profiles of the monomers (1, 2, and SP) and SPA-B (m:n:o=0.65:0.35:1.04, IEC 1.58 mequiv g^{-1}).

Table 1. Physical Properties of SPA Membranes

Sample	1(m) : 2 (n) : SP(o)	GPC (kDa)[a]		IEC (mequiv g^{-1})	
		M_n	M_w	Targeted[b]	Titrated[c]
A	0.50 : 0.50 : 1.04	61	134	1.7	1.61
	0.50 : 0.50 : 2.14	77	153	2.8	2.55
	0.50 : 0.50 : 3.17	93	161	3.4	3.18
B	0.65 : 0.35 : 1.04	64	139	1.7	1.58
	0.65 : 0.35 : 2.14	88	168	2.8	2.51
	0.65 : 0.35 : 3.17	104	183	3.4	3.11
C	1 : 0 : 1.10	13	64	1.7	1.52
	1 : 0 : 1.85	5	34	2.5	-[e]

[a] Determined by GPC (DMF containing 0.01 M LiBr was used as eluent). [b] Calculated from the feed monomer compositions assuming 100% conversion. [c] Obtained from titration. [d] Unavailable because a membrane was not obtained.

SPA-A and -B terpolymers provided thin, bendable, and brown membranes by casting from DMSO solution. SPA-B membranes were transparent while SPA-A membranes were slightly turbid, reflecting the lower solubility of the latter terpolymers containing more alkylene groups. Similar behavior was observed in our previously reported ammonium containing copolymers. Because of its lower molecular weight, SPA-C with higher IEC (2.5 mequiv g^{-1}) did not give a self-standing membrane. The IECs of the membranes were determined by acid-base titration. The resulting IEC values were only slightly lower (up to ca. 7%) than those calculated from the feed monomer ratios. It should be noted the high IEC values (> 2.0 mequiv g^{-1}) were achievable by introducing alkylene groups. The copolymerization of 1 and SP did not give high enough molecular weight copolymers to form self-standing membranes when the targeted IECs were higher than > 2.0 mequiv g^{-1} (results not shown).

2.4.2. Morphology

Figure 16 shows TEM images of SPA-A and SPA-B membranes stained with Pb^{2+} ions. The black domains are related with hydrophilic domains containing stained sulfonic acid groups. SPA-B (IEC = 1.58 mequiv g^{-1}) membrane with larger content of perfluoroalkylene groups than SPA-A (IEC = 1.61 mequiv g^{-1}) membrane exhibited somewhat more distinct phase-separated morphology. In addition, the hydrophilic clusters were more interconnected for SPA-B than for SPA-A. The average sizes of the hydrophilic and hydrophobic clusters were 3.6 nm and 3.0 nm for SPA-A, and 5.3 nm and 3.0 nm for SPA-B, respectively. The hydrophilic/hydrophobic difference of the components was more pronounced in SPA-B than in SPA-A, which must be responsible for such morphological differences. In the TEM images of SPA-B with higher IECs (2.51 and 3.11 mequiv g^{-1}), larger hydrophilic clusters (~ ca. 8 nm) were observed presumably because of the larger content of the ionic groups. Compared to the SPAF membrane with lower IEC (1.59 mequiv g^{-1}), the hydrophilic/hydrophobic domain sizes were similar but their interfaces were less distinct probably because of less hydrophobicity of the alkylene groups as the third component than the perfluoroalkylene groups.

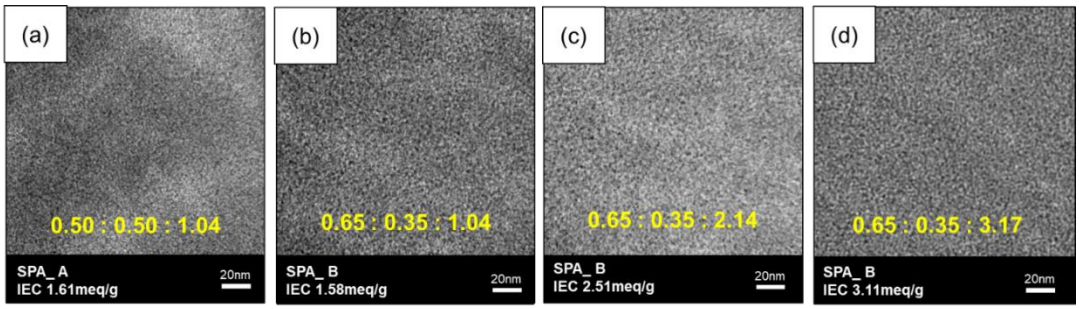

Monomer 1(m) : Monomer 2(n) : SP (o)

Figure 16. TEM images of SPA membranes stained with Pb^{2+} ions; (a) SPA-A membrane (IEC 1.61 mequiv g^{-1}), (b) SPA-B membrane (IEC 1.58 mequiv g^{-1}), (c) SPA-B membrane (IEC 2.51 mequiv $g^{-1)}$ and (d) SPA-B membrane (IEC 3.11 mequiv g^{-1}), respectively. The ratios in the images represent the feed monomer ratios.

In Figure 17, SAXS profiles of SPA-B membranes were measured at 30 - 90% relative humidity (RH) and 80°C. While SPA-B (IEC 3.0 mequiv g^{-1}) are no remarkable peaks at lower q vector, SPA-B (IEC 1.5 mequiv g^{-1}) and SPA-B (IEC 2.5 mequiv g^{-1}) membranes exhibited two peaks clearly decreasing peak at q vector = ca.0.1~0.3 nm^{-1} as dependence and slightly increasing peak at q vector = ca. 1 nm^{-1}, respectively, when increased %RH condition. According to that, lower q would be explained as matrix knee, hydrophobic domains, and higher q would be as ionic domains, hydrophilic, due to its dependency on relative humidity. As comparison with SPAF as reference, SPAF had shown no noticeable hydrophobic domains but probably structure containing alkyl group influences on well-developed hydrophobic domains. The d spacing of SPA-B > ca. 6 - 7 nm is show under higher humidity 90 %RH and bigger than SPAF membrane.

2.4.3. Proton conductivity and water uptake

Figure 18 shows proton conductivity and water uptake of SPA membranes at 80 °C as a function of RH. For reference, data for Nafion NRE212 membrane is also included. Water uptake and proton conductivity increased with increasing IEC for the SPA membranes. The water uptake of SPA-A and SPA-B membranes with similar IECs was comparable at a wide range of humidity, indicating minor effect of the composition of the hydrophobic components on the water affinity of the membranes. In other words, the sulfonic acid groups were hydrated to the similar levels in both series of the membranes. Despite their similar water affinity, SPA-B membranes exhibited slightly higher proton conductivities than those of SPA-A membranes. As discussed with the TEM images above, SPA-B

contained more interconnected ionic channels which should be responsible for higher proton conductivity. SPA-C membrane (1.52 mequiv g^{-1}) without alkylene groups in the main chain exhibited higher proton conductivity than those of SPA-A and -B membranes, in particular, at low humidity. The high IEC SPA-A (3.18 mequiv g^{-1}) and -B (3.11 mequiv g^{-1}) membranes exhibited comparable or higher proton conductivity compared to Nafion NRE 212 membrane at a wide range of humidity. These membranes outperformed SPA-C (1.59 mequiv g^{-1}) membrane; the proton conductivities of SPA-A, SPA-B, and SPA-C membranes were 2.3, 1.8, 3.2 mS cm^{-1} at 30% RH, respectively. Temperature dependence of water uptake and proton conductivity of SPA-B (IEC 2.51 mequiv g^{-1}) membrane was measured (Figure 19). The membrane retained its high conductivity up to 120 ºC while lost water uptake slightly.

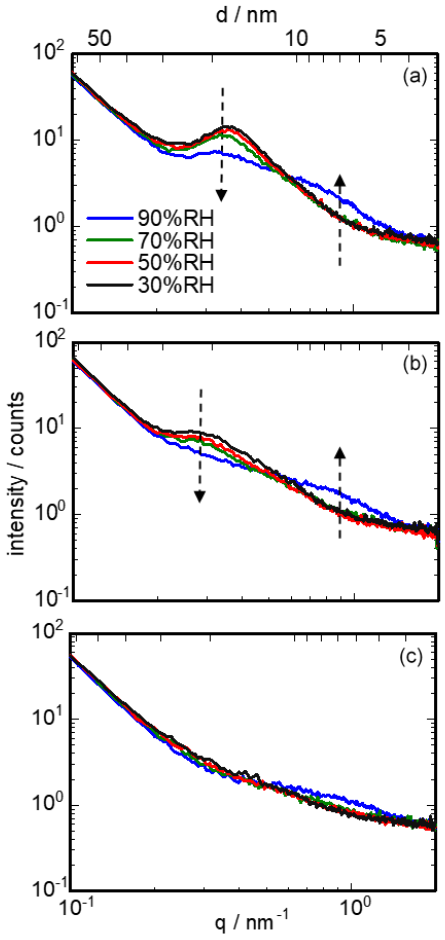

Figure 17. SAXS profiles for SPA-B membrane (a) IEC 1.5 mequiv g^{-1}, (b) IEC 2.5 mequiv g^{-1}, and (c) IEC 3.0 mequiv g^{-1}as a function of the scattering vector (q) value at relative humidity from 90 to 30%RH and 80°C. The dashed arrows indicated increasing humidity.

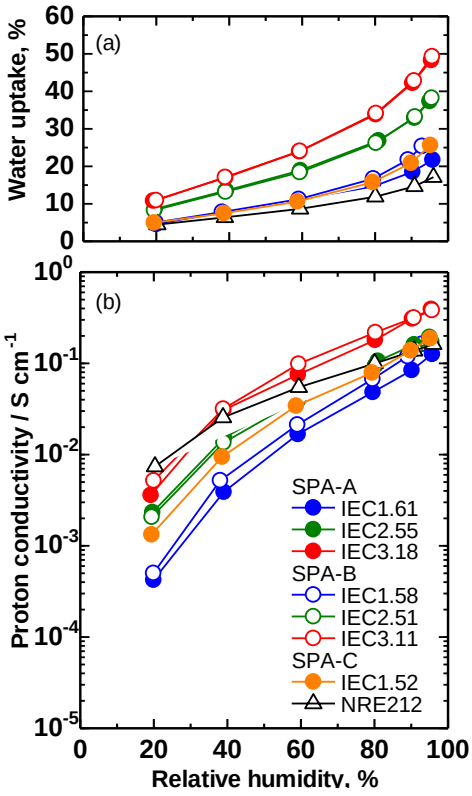

Figure 18. Humidity dependence of (a) water uptake and (b) proton conductivity of SPA and Nafion NRE212 membranes at 80 ºC.

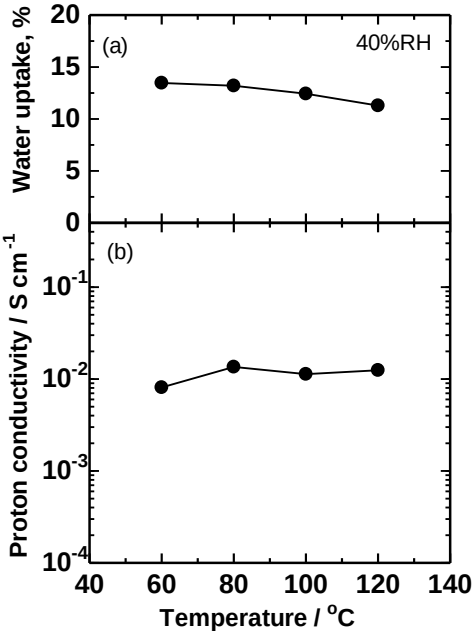

Figure 19. Temperature dependence of (a) water uptake and (b) proton conductivity of SPA-B (IEC 2.51 mequiv g^{-1}) membrane at 40% RH.

2.4.4. Mechanical properties

Humidity dependence of the storage modulus (E'), the loss modulus (E''), and tan δ (= E''/E') of the SPA membranes was investigated by dynamic mechanical analysis (DMA) at 80 ºC, as shown in Figure 20. SPA-A and SPA-B membranes exhibited similar viscoelastic properties without obvious transition behavior under the given conditions. The storage modulus decreased with increasing humidity for both series of the membranes, suggesting that absorbed water molecules soften the membranes. SPA-C membrane showed larger loss in E' and E'' at high humidity compared to those of SPA-A and -B membranes due to lower molecular weight than those of SPA-A and -B. As a result of this, the alkylene groups in the main chain were likely to mitigate the effect of water on the viscoelastic properties because of the ease in approaching higher molecular weight.

Figure 21 shows tensile test results (stress/strain curves) of SPA membranes at 80 ºC and 60% RH. SPA-A and SPA-B membranes exhibited similar elongation properties with the Young's moduli (0.9 - 2.5 GPa and 0.5 - 2.5 GPa), yield strengths (7.6 - 15 MPa and 4.9 - 12 MPa), and tenstile strains (15 - 81% and 12 - 99%), respectively, depending on their IEC. Briefly, as increasing the IEC value, the maximum strain decreased and the Young's modulus and yield strength increased (Table 2). Compared to SPA-C membrane (1.52 mequiv g^{-1}), SPA-A and -B membranes with similar IEC (1.61 and 1.58 mequiv g^{-1}, respectively) exhibited higher Young's moduli, higher yield strengths, and comparable maximum strains, indicating that the alkylene groups in the main chain enhanced the mechanical properties. The results are in agreement with the DMA data.

Table 2. Summary of Tensile Test Results of SPA-A, -B, and -C Membranes.

Membrane	IEC (mequiv g^{-1})	Maximum strain (%)	Young's modulus (GPa)	Yield strength (MPa)
SPA-A	1.61	80.6	0.09	7.6
	2.55	26.6	0.27	14.6
	3.18	14.5	0.25	15.0
SPA-B	1.58	98.7	0.05	4.9
	2.51	25.7	0.22	11.1
	3.11	11.5	0.25	12.0
SPA-C	1.52	89.0	0.03	3.7

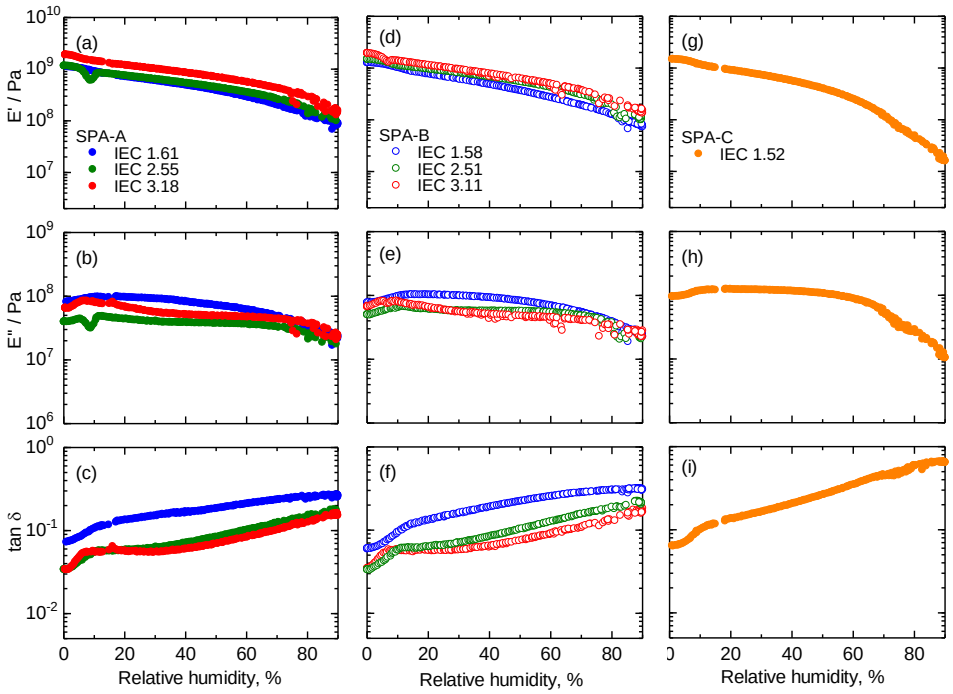

Figure 20. Dynamic mechanical analyses of SPA membranes at 80 ºC as a function of the relative humidity; (a) E', (b) E'' and (c) tan σ for SPA-A, (d) E', (e) E'' and (f) tan σ of SPA-B and (g) E', (h) E'' and (i) tan σ of SPA-C, respectively.

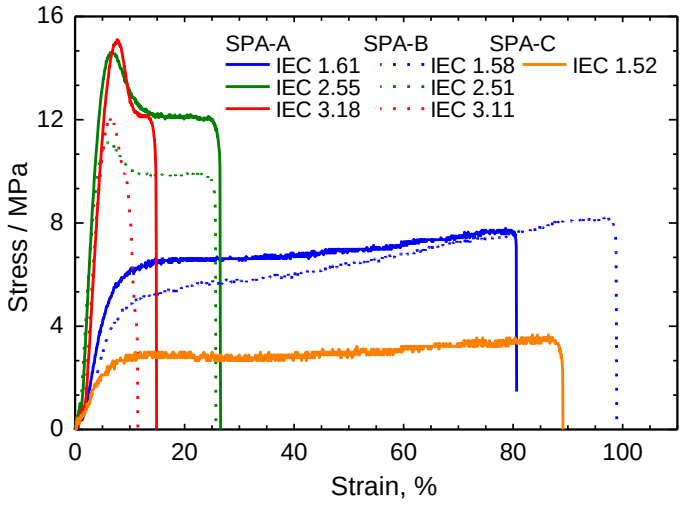

Figure 21. Stress versus strain curves of SPA membranes at 80 ºC and 60% RH.

2.4.5. Fuel Cell Performance

Because of the balanced properties of water uptake, proton conductivity, mechanical properties, and their humidity dependence, SPA-B (IEC 2.51 mequiv g^{-1}) was chosen for fuel cell evaluation. A membrane electrode assembly (MEA) was prepared from the SPA-B membrane (29 μm thick) with catalyst layers consisting of Pt/CB catalyst and Nafion binder for both the anode and the cathode. To evaluate the hydrogen permeability of the membrane, linear sweep voltammograms (LSVs) were measured at 80 ºC supplying humidified hydrogen and nitrogen to the anode and cathode, respectively, (Figure 22) prior to the performance evaluation. The oxidation current density of the permeated hydrogen was very small (ca. 3 μA cm^{-2}) at 30% RH and higher (0.42 - 0.50 mA cm^{-2}) at 100% RH. The hydrogen permeability of the SPA-B membrane was comparable to that of the SPAF membrane (0.40 mA cm^{-2} at 100% RH, 28 μm thick) and much smaller than that of Nafion NRE 212 membrane (1.45 mA cm^{-2} at 100% RH, 25 μm thick).

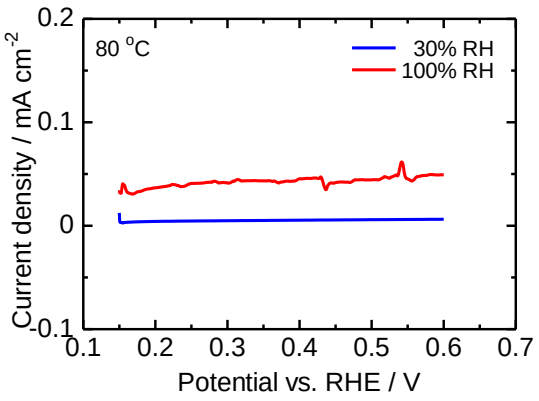

Figure 22. Linear sweep voltammograms (LSVs) of fuel cell with SPA-B (IEC = 2.51 mequiv g^{-1}) membrane at 80 ºC, 30% RH and 100% RH.

Figure 23 shows polarization curves (ohmic (IR) drop-included) and ohmic resistances of the fuel cell with the SPA-B membrane operated with hydrogen and oxygen or air at 80 ºC, 100% RH and 30% RH. The open circuit voltages (OCVs) were 0.99 V (oxygen, 100% RH), 0.96 V (air, 100% RH), 1.01 V (oxygen, 30% RH), and 0.97 V (air, 30% RH), respectively. The high OCV values support low hydrogen permeability of the membrane as suggested by LSVs. At 100% RH, the ohmic resistance was 0.05 Ω cm^2 both with oxygen and air, which was only slightly higher than that (0.02 Ω cm^2) calculated from the proton conductivity (Figure 18b) and the thickness of the membrane. The results indicate reasonably good interfacial contact between the SPA-B membrane and the Nafion-based

catalyst layer. At 30% RH, the ohmic resistance was ca. 0.4 Ω cm^2 at OCV and decreased with increasing the current density to 0.11 Ω cm^2 with oxygen and 0.26 Ω cm^2 with air, which were lower than that (0.51 Ω cm^2) calculated from the proton conductivity and the thickness. The lower ohmic resistances in the operating fuel cell resulted from the back-diffusion of water from the cathode to the membrane. The effect was more pronounced with oxygen than with air since the oxygen flow rate (0.038 mL min^{-1} at 1 A cm^{-2}) was slower than air flow rate (0.182 mL min^{-1} at 1 A cm^{-2}) to have the same oxygen utility (40%). The ohmic resistance of SPA-B cell at 30% RH was smaller than that (0.33 Ω cm^2 with air) of SPAF (IEC = 1.59 mequiv g^{-1})-cell due to the former's higher IEC and higher proton conductivity.

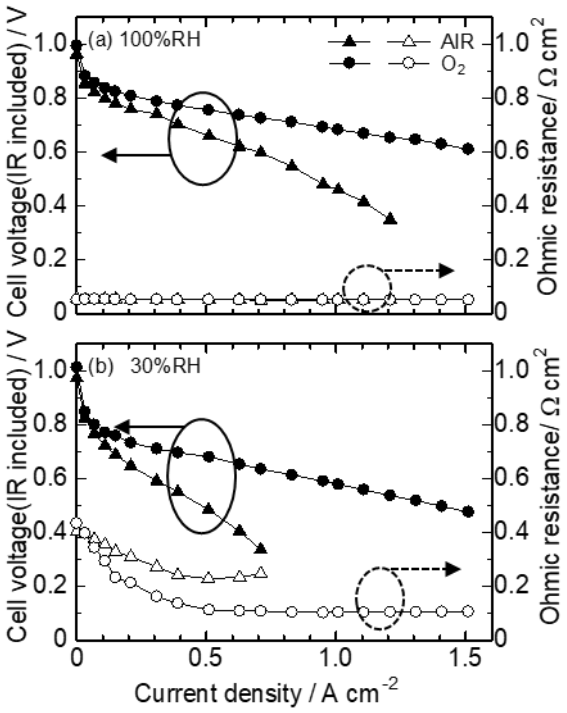

Figure 23. IR-included polarization curves and ohmic resistances of fuel cell with SPA-B membrane (IEC = 2.51 mequiv g^{-1}) at 80 ºC under humidity conditions (a) 100% and (b) 30% RH.

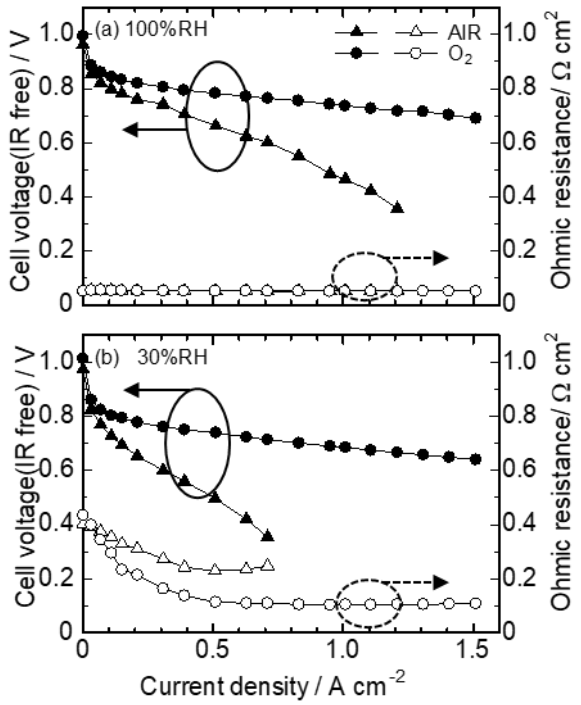

Figure 24. IR-free polarization curves and ohmic resistances for SPA-B cell (IEC = 2.51 mequiv g^{-1}) at 80 ºC under humidity conditions (a) 100% and (b) 30% RH.

In order to evaluate the compatibility of the SPA-B and Nafion membrane and the Nafion-based catalyst layer in more detail, IR-corrected IV curves were plotted (Figure 24 and 25) and mass activities (MAs) of the Pt catalysts in the cathode at 0.85 V were calculated therefrom. The MAs of the SPA-B cell with air were 73 A g^{-1} at 100% RH which were lower than those of the SPAF cell (102A g^{-1} at 100% RH) and the Nafion cell (113A g^{-1} at 100% RH) under the same operating conditions. However, The MAs of the SPA-B cell with air were 58 A g^{-1} at 30% RH, respectively, which were slightly higher than those of the SPAF cell (51 A g^{-1} at 30% RH) and the Nafion cell (41 A g^{-1} at 30% RH) under the same operating conditions. Despite its higher proton conductivity and similarly phase-separated morphology, the SPA-B cell exhibited lower mass transport capability at the interface of the membrane/cathode catalyst layer than that of the SPAF cell, especially under higher RH test conditions. This could be explained by different degrees of water absorbability, which can cause an interfacial disconnect between the catalyst layer and the SPA-B membrane. The SPA-B cell shows comparable performance under lower RH test conditions. Less distinct hydrophobic/hydrophilic phase separations would be responsible, in particular, at low humidity where proton transport to the catalyst surface became more crucial.

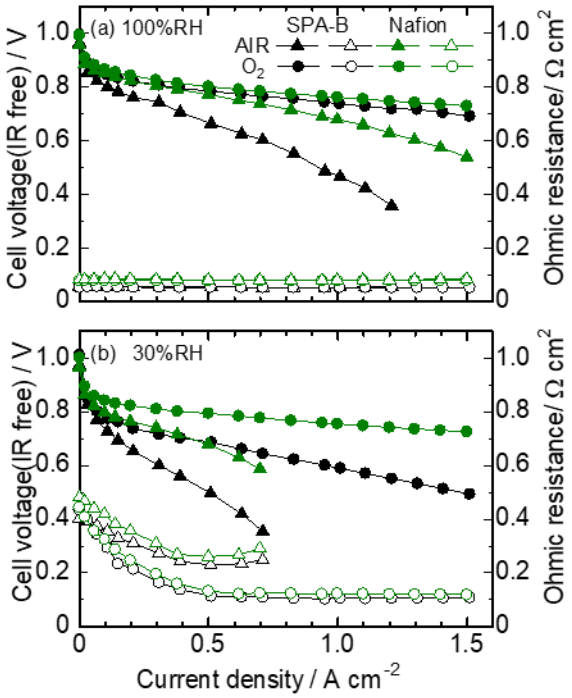

Figure 25. IR-free polarization curves and ohmic resistances for SPA-B cell (IEC = 2.51 mequiv g^{-1}) and Nafion 212 at 80 ºC under humidity conditions (a) 100% and (b) 30% RH.

To evaluate the durability of the SPA-B membrane, an OCV hold test was carried out with hydrogen and air (Figure 26). The OCV was initially 0.98 V and decreased to 0.86 V after 1000 h with an average decay of -120 μV/h. No sudden drop of OCV was observed during the test, indicating no serious damage on the membrane such as pinholes. After the OCV hold test for 1000 h, the I-V performance was re-evaluated under the same operating conditions (Figure 27). The OCV decreased after the test from 0.99 V to 0.95 V (oxygen, 100% RH), 0.96 V to 0.91 V (air, 100% RH), 1.01 V to 0.85 V (oxygen, 30% RH), and 0.97 V to 0.90V (air, 30% RH), respectively. The post-OCV hold test cell exhibited lower fuel cell performances than those of the pristine membrane cell. The loss in the performance, however, was not significant but rather minor with oxygen at 100% RH, followed by air at 100% RH and oxygen at 30% RH, and air at 30% RH. Since the ohmic resistances of the post-OCV hold test cell were similar to those of the pristine membrane (except for air at 30% RH), the lowered fuel cell performances were more likely caused by the degradation of the Nafion-based catalyst layers. This idea was supported by the IR-corrected curves in Figure 28, where the lower cathode performances were confirmed with the post-OCV hold test cell. The results support minor degradation of the SPA-B membrane under the test conditions.

The fuel cell was disassembled, and the SPA-B membrane was recovered by carefully removing the catalyst layers from both sides of the membrane to analyze the changes in the molecular weight and chemical structure. The recovered SPA-B membrane was still bendable. The GPC curves of the post-test SPA-B shifted to the longer retention time resulting in the lower number-averaged molecular weight (Mn = 30 kDa) with larger dispersity (PDI = 7.0) than those of the pristine SPA membrane (Figure 29). ^{19}F NMR spectrum did not show practical changes suggesting chemical robustness of the perfluoroalkylene groups (Figure 30a). In contrast, the ^{1}H NMR spectrum of the post-test SPA-B membrane differed from that of the pristine membrane (Figure 30b). The peaks assignable to the aliphatic protons (no. 9 - 11) and aromatic protons (no. 5 - 8 and 12 - 14) were smaller for the post-test membrane. The results suggest some degradation of the components derived from the monomer 2, accountable for slightly higher ohmic resistance of the post-test fuel cell with air at 30% RH.

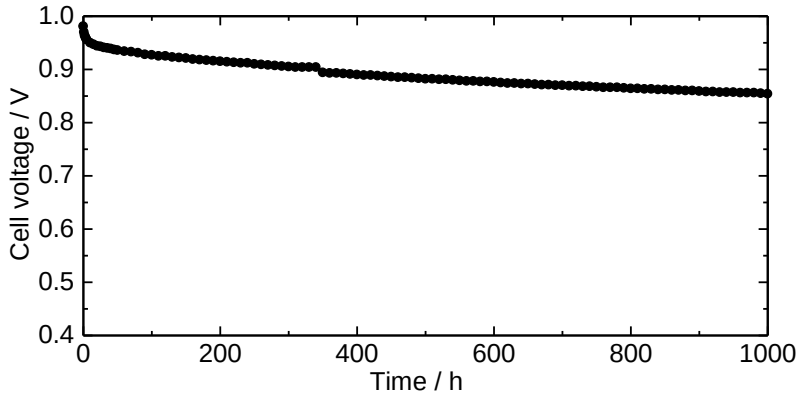

Figure 26. OCV hold test of SPA-B cell (IEC = 2.51 mequiv g^{-1}) at 80 ºC and 30% RH.

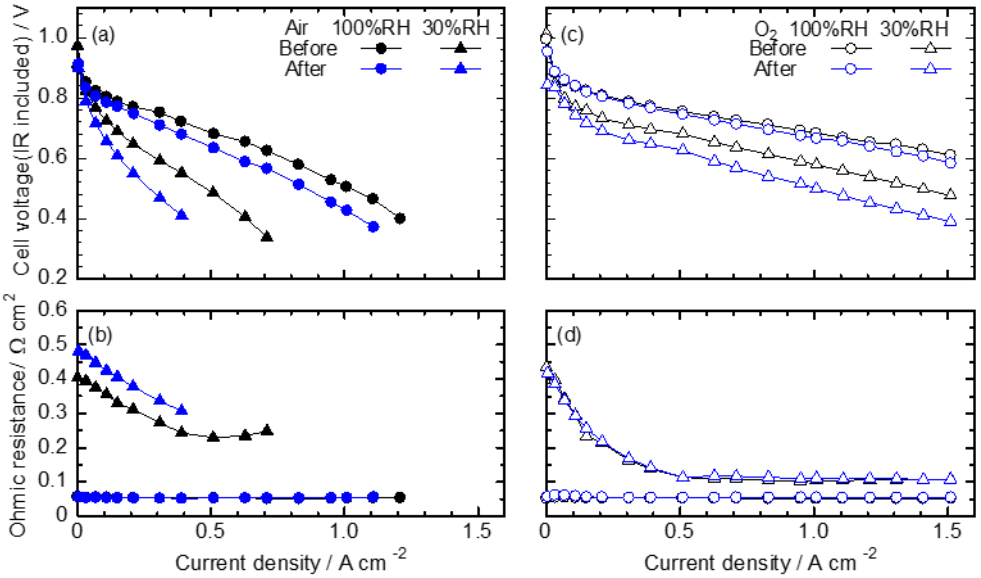

Figure 27. IR-included polarization curves and ohmic resistances of the fuel cell of SPA-B membrane before and after the OCV hold test; (a) and (b) with air and (c) and (d) with oxygen at 80°C, 100% and 30%RH.

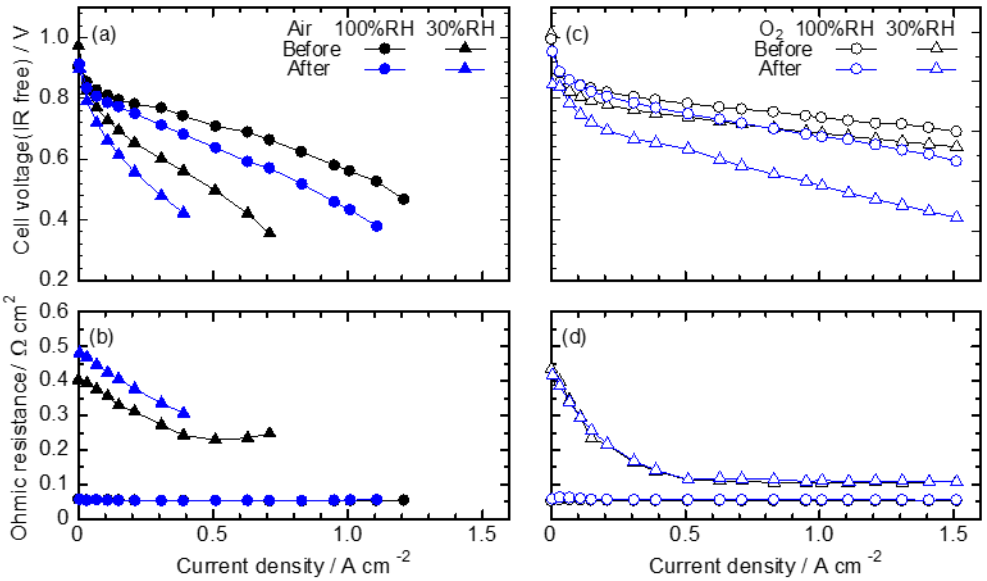

Figure 28. IR-free polarization curves and ohmic resistances of the fuel cell of SPA-B membrane before and after the OCV hold test; (a) and (b) with air and (c) and (d) with oxygen at 80°C, 100% and 30%RH.

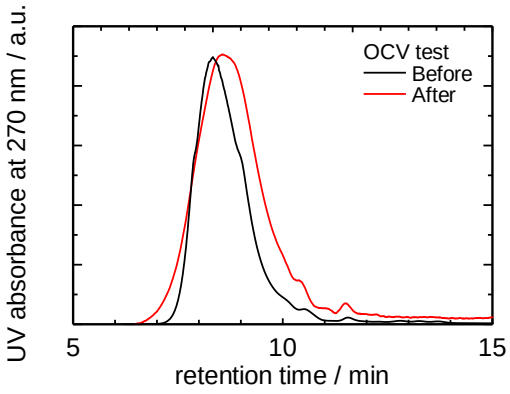

Figure 29. GPC profiles of SPA-B membrane before and after the OCV hold test.

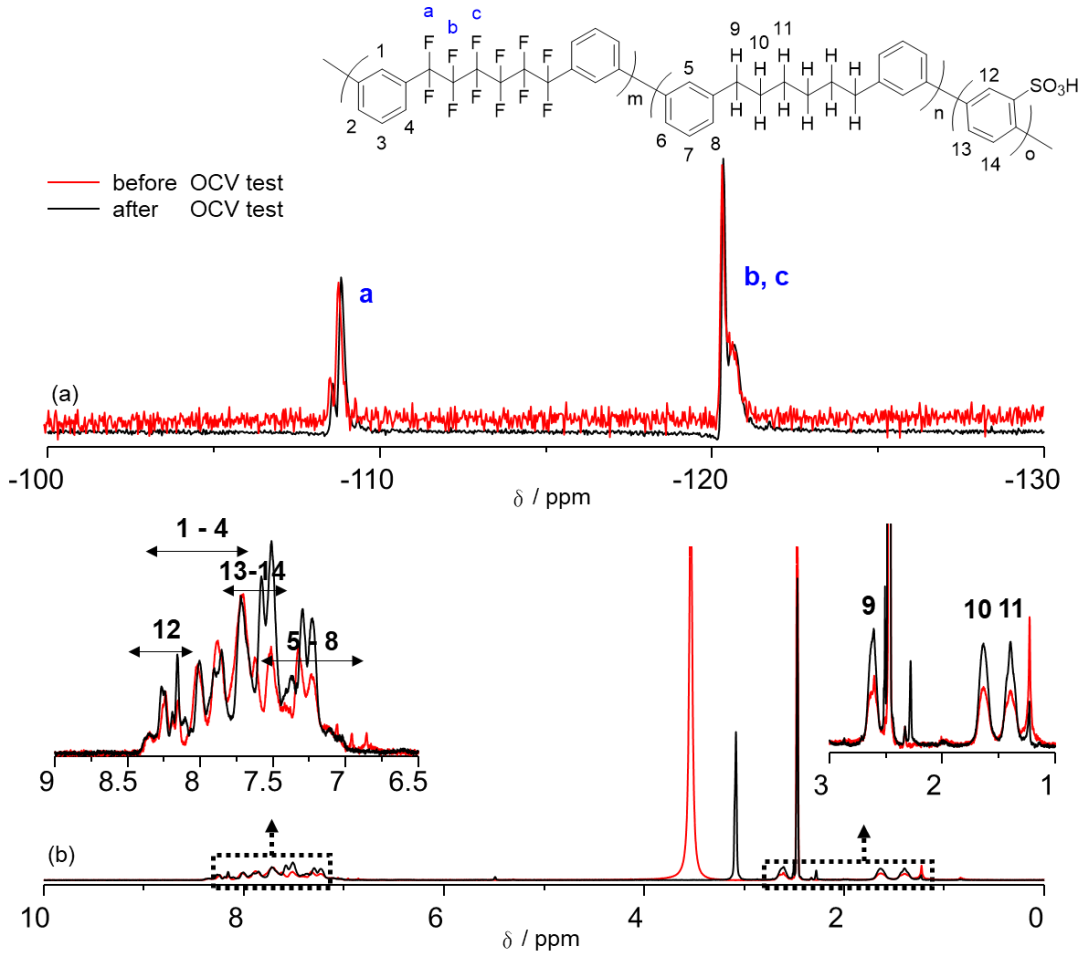

Figure 30. (a) ^{19}F and (b) ^{1}H NMR spectra of SPA-B membrane before and after the OCV hold test in DMSO-d_6 at 80 °C.

2.5. Conclusions

We have successfully synthesized two types of sulfonated terpolymers (SPA) containing perfluoroalkylene and alkylene groups to investigate the effect of these (perfluorinated) aliphatic groups on the membrane and interface properties. Both series of terpolymers provided bendable membranes by solution casting. Introducing alkylene groups enabled higher IEC membranes than the previous sulfonated copolymer (SPAF) membranes without alkylene groups. The effect of the aliphatic groups on the membrane properties was significant. Because of the less hydrophobic nature of the alkylene groups than the perfluoroalkylene groups, the hydrophilic/hydrophobic phase-separated morphology of SPA-A membranes with higher alkylene content was less distinct. SPA-B membranes exhibited slightly higher proton conductivity and similar water uptake compared to those of SPA-A membranes reflecting more developed morphology of the former ones with better interconnected ionic channels. Because of IEC higher than that of SPAF membrane, SPA membranes showed much higher proton conductivity. The alkylene groups in the main chain also impacted on the mechanical properties. SPA-A and -B membranes exhibited higher Young's moduli, higher yield strengths and comparable maximum strains compared to those of SPA-C membrane. The SPA-B membrane showed very low hydrogen permeability as suggested by low hydrogen oxidation current densities in LSVs and high OCVs in a fuel cell. The ohmic resistance of the fuel cell was reasonable for high proton conductivity of the SPA-B membrane. The compatibility of the SPA-B membrane with Nafion-based catalyst layers was not as good as that of SPAF membrane probably because of the inefficient mass transport capability at their interfaces in particular at low humidity. The OCV hold test of the fuel cell revealed high oxidative durability of the SAP-B membrane with small loss in OCV value (the average decay of -120 μV/h) for 1000 h. The post-test durability analyses of the SPA-B membrane suggested small but not severe degradation in the alkylene groups in the main chain. By tuning the alkylene chain length and/or terpolymer composition, incompatibility with the catalyst layers and chemical vulnerability would be mitigated.

References

[1] M. A. Hickner, H. Ghassemi, Y. S. Kim, B. R. Einsla, J. E. McGrath, *Chem. Rev.*, 2004, 104, 4587-4612.

[2] H. Zhang, P. K. Shen, *Chem. Rev.*, 2012, 112, 2780-2832.

[3] T. Higashihara, K. Matsumoto, M. Ueda, *Polymer*, 2009, 50, 5341-5357.

[4] J. Miyake, K. Miyatake, *Polym. J*, 2017, 49, 487-495.

[5] J. Ahn, H. Lee, T. Yang, C. Kim and B. Bae, *J. Polym. Sci. Part A: Polym. Chem.*, 2014, 52, 2947-2957

[6] C. H. Park, C. H. Lee, M. D. Guiver and Y. M. Lee, *J. Prog. Polym. Sci.*, 2011, 36, 1443-1498

[7] M. A. Hickner, H. Ghassemi, Y. S. Kim, B. R. Einsla and J. E. McGrath, *Chem. Rev.*, 2004, 104, 4587-4612

[8] J. Miyake, R. Taki, T. Mochizuki, R. Shimizu, R. Akiyama, M. Uchida and K. Miyatake, *Sci. Adv.*, 2017, 3, eaao0476

[9] T. Mochizuki, M. Uchida, K. Miyatake, *ACS Energy Lett*., 2016, 1, 348-352.

[10] H. Ono, J. Miyake, S. Shimada, M. Uchida, K. Miyatake, *J. Mater. Chem. A*, 2015, 3, 21779-21788

[11] M. Shimada, R. Akiyama, H. Ono, J. Miyake, K. Miyatake, *Chem. Lett.*, 2017, 46, 374-377

Chapter 3. Sulfonated aromatic polymers containing hexafluoroisopropylidene groups

3.1 Introduction

More recently, our laboratory has developed a simpler version of sulfonated polyphenylene composed only of phenylene rings and sulfonic acid groups. [1] By carefully optimizing the m-/p- composition and sulfonic acid concentration, we proved that sulfonated polyphenylene (SPP-QP, Figure 31) with a very simple polymer structure provided thin membranes with bendability, high proton conductivity, and excellent chemical stability. The SPP-QP membrane functioned well in an operating hydrogen/oxygen fuel cell with high performance and durability.

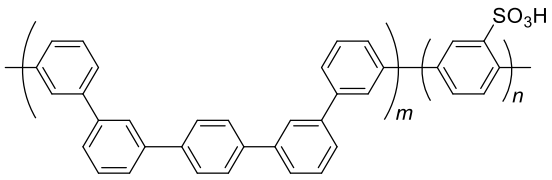

Figure 31. Chemical structures of sulfonated poly(phenylene) (SPP-QP) composed only of phenylene rings and sulfonic acid groups.

The results prompted us to further investigate the polymer structure for better performing proton conductive aromatic ionomers. In the present research, I replaced quinquephenylene groups (five consecutive phenylene rings in SPP-QP) with hexafluoroisopropyl biphenylene groups, since the latter contain an even simpler structure and could be prepared in a single step in high yield from the commercially available inexpensive chemicals (e.g., bisphenol-AF). We report herein synthesis and characterization of a novel series of sulfonated phenylene polymers containing hexafluoroisopropylidende groups in the main chain. Their properties, including fuel cell performance and durability, are compared, in detail, with those of our SPP-QP membranes.

3.1. Measurements

^{1}H and ^{19}F NMR spectra were measured a JEOL JNM-ECA ECX500 using deuterated dimethyl sulfoxide (DMSO-$_{d6}$) containing 1 vol% tetramethylsilane as internal reference.

The molecular weight of the monomers and copolymers was measured via gel permeation chromatography (GPC) equipped with a Jasco 805 UV detector. Dimethylformamide (DMF)

containing 0.01 M lithium bromide (LiBr) was used as the eluent. Shodex KF-805L and SB-803HQ columns were used for the measurement of polymers and monomers, respectively. Molecular weight was calibrated using standard polystyrene samples.

Ion exchange capacity (IEC) of the membranes was measured by titration at r.t. A piece of dry membrane in acid form was immersed into 2M NaCl aqueous solution for at least 24 h. The released HCl in the solution was titrated with 0.01 M NaOH aqueous solution. The IEC was calculated using the following equation; IEC (mequiv. g^{-1}) = $\Delta V_{NaOH} \times C_{NaOH} / W_d$, where ΔV_{NaOH} is the consumed volume of NaOH solution, C_{NaOH} is the concentration of NaOH solution, and Wd is the weight of the dry membrane.

Morphology of the membranes was analyzed by transmission electron microscopy (TEM). For TEM observation, the membranes were stained with lead ions (Pb^{2+}) by ion exchange of sulfonic acid groups in 0.5M $Pb(OAc)_2$ aqueous solution, rinsed with deionized water, and dried in a vacuum oven for 12h. The stained samples were embedded in epoxy resin, sectioned into 50nm slices with a Leica microtome Ultracut UCT, collected by copper grids, and then investigated with a Hitachi H-9500 TEM at an acceleration voltage of 200kV.

The SAXS measurement was conducted using a Rigaku NANO-Viewer diffractometer equipped with a temperature/humidity-controlled chamber. The membrane was equilibrated for at least 2h under each humidity condition from 30% to 90% relative humidity (RH) at 80 ºC.

Proton conductivity and water uptake were measured in a temperature and humidity controllable chamber at 80ºC from 95% to 20% RH. Ion conducting resistances (R) were determined from the impedance plot. The proton conductivity (σ) was calculated according to the following equation; σ =L/(S × R), where L, S, and R are the thickness of the membrane, the area of the electrodes, and the resistance of the membrane, respectively.

Dynamic mechanical analyses (DMA) of the membranes (0.5cm × 3cm) were carried out with an ITK DVA-225 dynamic viscoelastic analyzer at 80 ºC from 0% to 90% RH. The storage modulus (E'), loss modulus (E''), and tan σ (= E''/E') of the membranes were recorded.

Tensile strength of the membranes was measured in a temperature and humidity controllable chamber. Stress versus strain curves were obtained for samples cut into a dumbbell shape (DIN-53503-S3, 35mm × 6mm (total) and 12 mm × 2 mm (test area)). The measurement was conducted at 80 ºC and 60% RH at a stretching rate of 10 mm min^{-1}.

Hydrogen and oxygen permeability of the membranes was measured with a GTR-Tech 20XFYC

gas permeation measurement apparatus equipped with a Yanaco G2700T gas chromatograph (GC) with a Porapak Q column and a thermal conductivity detector. Argon and helium were used as carrier gases for the measurement of hydrogen and oxygen, respectively. Membranes were placed in the center of the cells having gas inlet/outlet on both sides of membranes. The test gas was supplied to one side of the membranes and the carrier gas was supplied to the other side of membranes. The same humidity conditions were applied to both test and carrier gases to ensure homogeneous wetting of the membranes. Then, flow gas was sampled and subjected to the GC to quantify the test gas permeated through the membrane. The gas permeability coefficient of the membranes Q [cm^3 (STP) cm cm^{-2} s^{-1} $cmHg^{-1}$] was calculated by the following equation: $Q = 273/T \times 1/A \times B \times 1/t \times l \times 1/(76 - P_{H_2O})$, where T (K) is the absolute temperature, A (cm^2) is the permeation area, B (cm^3) is the volume of permeated test gas, t (s) is the sampling time, l (cm) is the thickness of the membrane, and P_{H_2O} (cmHg) is the water vapor pressure.

3.2. Experimental

3.2.1. Materials

2,5-Dichlorobenzenesulfonic acid dehydrate (SP) (TCI), 4,4'-(hexafluoroisopropylidene)diphenol (TCI), dichlorotriphenylphosphorane (Sigma-Aldrich), bis(1,5-cyclooctadiene)nikel(0) ($Ni(COD)_2$) (> 95%, Kanto Chemical), 2,2'-bipyridine (> 99%, Kanto Chemical), potassium carbonate (K_2CO_3) (Kanto Chemical), sodium chloride (NaCl) (Kanto Chemical), dimethyl sulfoxide (DMSO) (> 99%, Kanto Chemical), and toluene (> 99%, Kanto Chemical) were used as received. 2,2-Bis(4-chlorophenyl)hexafluoropropane (BAF) was synthesized according to the literature.[2]

3.2.2. Polymerization

A series of SBAF copolymers were synthesized as follows. A 100 mL three-neck flask was charged with 2,2-bis(4-chlorophenyl)hexafluoropropane (BAF, 0.2984 g, 0.8 mmol), 2,5-dichlorobenzenesulfonic acid dehydrate (SP, 0.3683 g, 1.4 mmol), K_2CO_3 (0.2322 g, 1.68 mmol), 2,2'-bipyridine (1.4498 g, 9.24 mmol), DMSO (6 mL), and toluene (6 mL). The mixture was heated in the temperature-controlled oil bath at 170 °C for 2 h with a Dean Stark trap under N_2. After azeotropic dehydration, the mixture was cooled to 80 °C. To the mixture, $Ni(COD)_2$ (1.2708 g, 4.62 mmol) was added. After the reaction at 80 °C for 3 h, the mixture was poured into large excess of 6 M HCl to precipitate the product. The crude product was washed with concentrated HCl and deionized water

several times. The copolymer was obtained by drying at 80 °C in a vacuum oven overnight in > 96% yield

3.2.3. Preparation of catalyst-coated membrane (CCM)

A catalyst paste was prepared by mixing Pt/CB catalyst (TEC10E50E, Tanaka Kikinzoku Kogyo K. K.), Nafion dispersion (IEC = 0.95 - 1.03 mequiv g^{-1}, D-521, Du Pont), deionized water, and ethanol by ball milling for 30 min. The mass ratio of Nafion ionomer to the carbon support (I/C) was adjusted to be 0.7. The catalyst-coated membrane (CCMs) was prepared by spraying the catalyst paste on both sides of SBAF membrane (IEC = 2.6 mequiv g^{-1}, 32 μm thick) by pulse swirl spray (PSS) technique. The CCM was dried at 60 °C overnight and hot-pressed at 140 °C and 1.0 MPa for 3 min. The geometric area and the Pt loading amount of the catalyst layer (CL) were 4.41 cm^2 and 0.5 mg cm^{-2}, respectively. The CCM was sandwiched by two gas diffusion layers and mounted into a cell which had serpentine flow channels on both the anode and the cathode sides.

3.3. Results and discussion

3.3.1. Synthesis of SBAF copolymers and membranes

A series of title copolymers, SBAF, were prepared by Ni(0)-promoted coupling reaction from BAF and SP monomers (Scheme 2). The feed comonomer composition was controlled to obtain copolymers with IEC ranging from 1.7 to 3.5 mequiv g^{-1}. The copolymerization reaction proceeded well at 80 °C in DMSO solution to provide the products in high yields (~ 94%). The resulting SBAF copolymers were soluble in polar organic solvents such as DMSO, DMAc, and NMP. SBAF copolymers were high-molecular-weight (Mw = 158 - 180 kDa, Mn = 42 - 66 kDa) with reasonable polydispersity (PDI = 2.7 - 3.7) as suggested by GPC measurement (Table 3 and Figure 32). ^1H and ^{19}F NMR spectra of the SBAF copolymers were well-assigned to the supposed chemical structure (Figure 33). The IEC values estimated from the integral ratios of the peaks in the ^1H NMR spectra were smaller than those calculated from the comonomer compositions, suggesting lower reactivity of SP monomer than BAF monomer. Casting from DMSO solution provided yellow transparent and flexible membranes of the SBAF copolymers. It should be noted that SBAF was composed solely of p-phenylene units in the main chain while in SPP-QP m-/p-=4/1 as isomeric composition was optimal in the phenylene units to obtain flexible membranes. Hexafluoroisopropylidene groups containing sp^3 hybridized carbon atoms were effective in improving membrane forming capability of sulfonated polyphenylenes. The

IEC values of the membranes obtained by acid/base titration were in fair agreement with those from the NMR spectra, indicating that the sulfonic acid groups functioned well as ion exchange groups in the membranes.

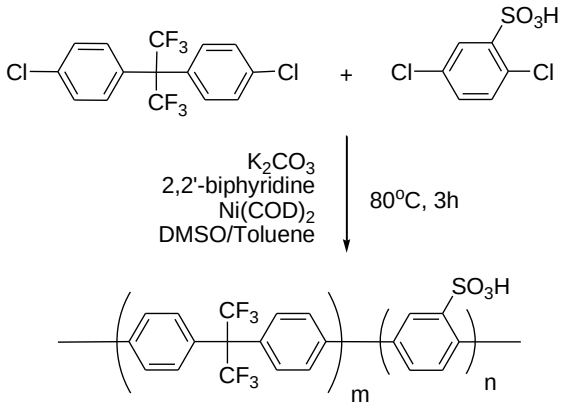

Scheme 2. Synthesis of SBAF copolymers

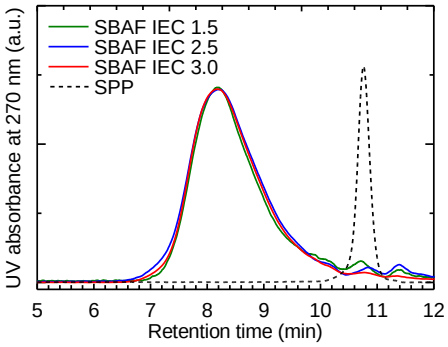

Figure 32. GPC profiles of SBAF copolymers.

Table 3. Composition, molecular weight, and ion exchange capacity (IEC) of SBAF copolymers.

No	Composition		IEC[a]	IEC[b]	IEC[c]	Molecular weight (kDa) [d]		
	m[a]	n[a]		(mequiv g^{-1})		M_n	M_w	PDI
1	0.8	0.6	1.7	1.4	1.5	42	158	3.7
2	0.8	1.4	3.0	2.3	2.5	66	180	2.7
3	0.8	1.9	3.5	2.7	3.0	62	171	2.7

[a] Calculated from the feed comonomer ratio. [b] Measured by NMR. [c] Measured by titration. [d] Measured by GPC

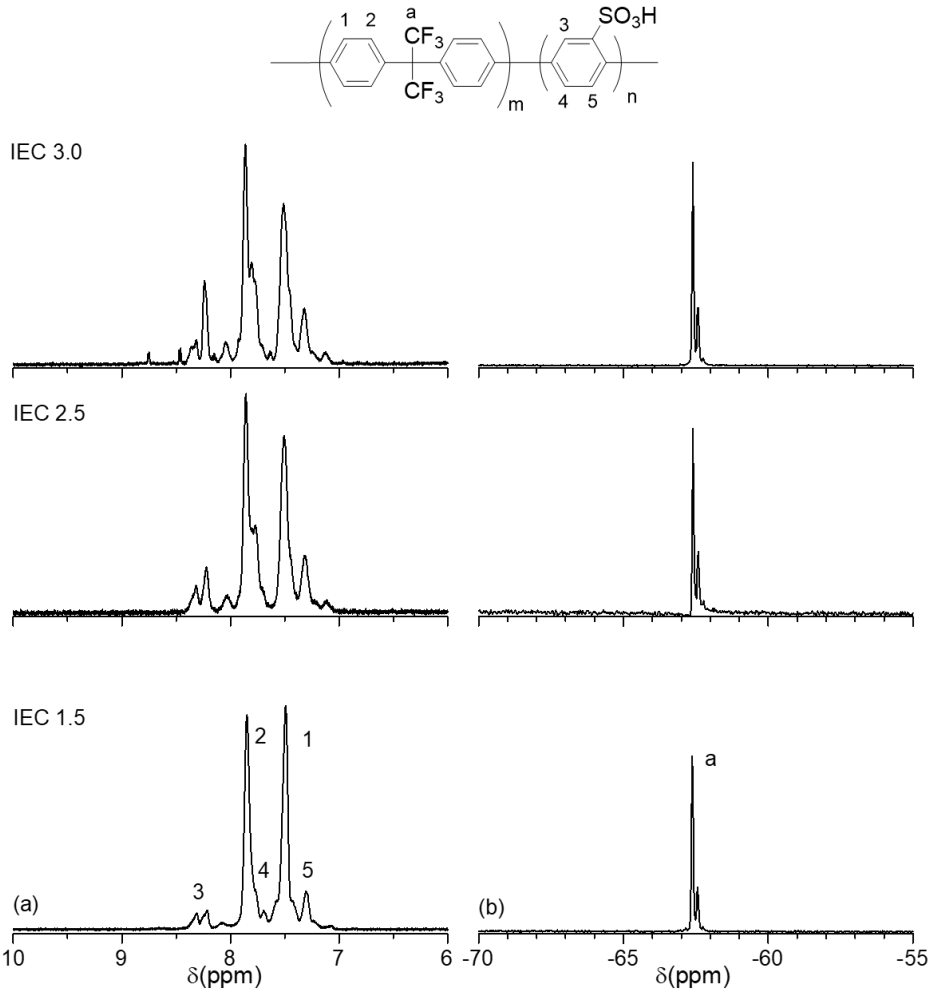

Figure 33. (a) ^{1}H and (b)^{19}F NMR spectra of SBPA terpolymer in DMSO-$_{d6}$ at 80 ºC.

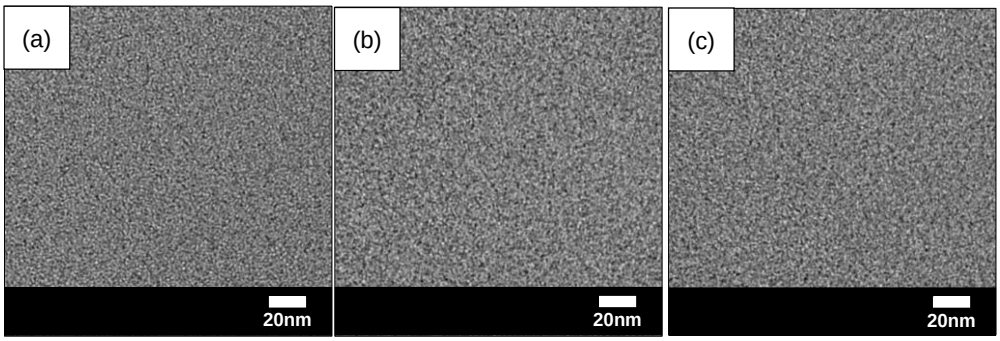

Figure 34. TEM images of SBAF membranes stained with Pb^{2+} ions; (a) IEC = 1.5 mequiv g^{-1}, (b) IEC = 2.5 mequiv g^{-1}, and (c) IEC = 3.0 mequiv g^{-1}, respectively.

3.3.2. Morphology

The TEM images were taken for three SBAF membranes stained with Pb^{2+} ions (Figure 34). The SBAF membranes exhibited well-developed phase separation between hydrophilic (dark) clusters and hydrophobic (bright) clusters. The phase-separation became more distinct and the cluster size became larger as increasing the IEC. The average sizes of the hydrophilic clusters calculated from the images were 2.9 nm for IEC = 1.5 mequiv g^{-1}, 3.3 nm for IEC = 2.5 mequiv g^{-1}, and 3.8 nm for IEC = 3.0 mequiv g^{-1}, respectively (the standard deviation value was 1.2 for three membranes). The morphology and the cluster sizes of SBAF membranes were similar to those of the SPP-QP membranes with comparable IECs suggesting that the QP and BAF groups as hydrophobic components contributed similarly to the phase-separation.

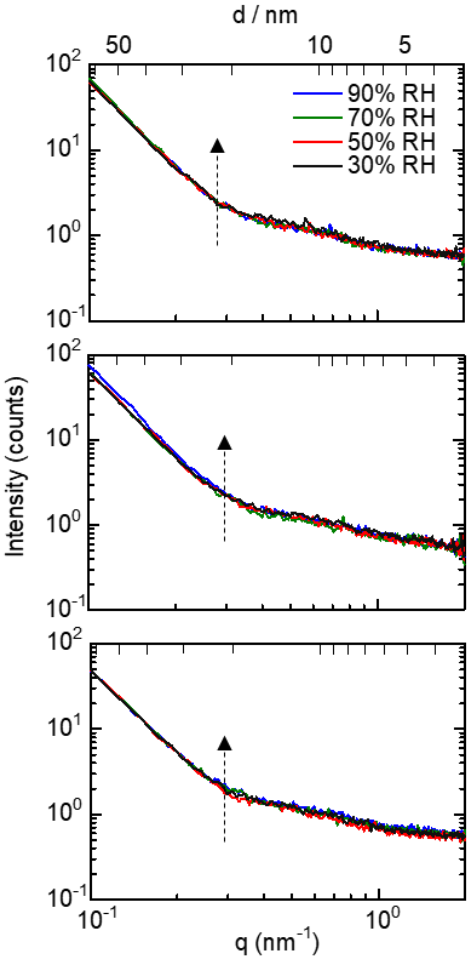

Figure 35. SAXS profiles for SBAF membranes (a) IEC = 1.5 mequiv g^{-1}, (b) IEC = 2.5 mequiv g^{-1}, and (c) IEC = 3.0 mequiv g^{-1} as a function of the scattering vector (q) value at relative humidity from 90% to 30% RH and 80 ºC. The dashed arrows indicate increasing humidity.

In order to investigate the effect of water on the morphology of SBAF membranes, small-angle X-ray scattering (SAXS) measurement was carried out at 80 °C with controlled humidity from 30 to 90% RH. In Figure 35, the scattered intensity is plotted as a function of the scattering vector (q). Three SBAF membranes with different IEC values exhibited very similar SAXS profiles with no obvious peaks and no humidity dependence. In contrast, SPP-QP membrane (IEC = 2.4 mequiv. g^{-1}) exhibited a clear ionomer peak at q = ca. 0.75 nm^{-1} which developed as increasing the humidity. Smaller BAF groups would not promote the formation of periodic structure when water molecules were included.

3.3.3. Proton conductivity and Water uptake

Humidity dependence of water uptake and proton conductivity of SBAF membranes was measured at 80°C (Figure 36). As expected, the water uptake of SBAF membranes increased by increasing humidity and IEC. Compared to SPP-QP membranes with comparable IECs, SBAF membranes showed slightly higher water uptake, in particular, at high humidity (Figure 37). Since the absorbed water did not contribute to the formation of periodic hydrophilic structure (as discussed with the above SAXS data), water molecules were possibly incorporated in the hydrophobic domains as well as in the hydrophilic domains due to the less pronounced hydrophilic/hydrophobic differences between the BAF and SP components than those in SPP-QP membranes. The degree of swelling of SBAF membrane (IEC = 2.5 mequiv g^{-1}) in water at r.t. was 30% (through-plane) and 20% (in-plane), respectively.

Proton conductivity of SBAF membranes exhibited similar humidity/IEC dependence to that of water uptake. SBAF membranes with IEC higher than 2.5 mequiv g^{-1} showed comparable or higher conductivity than that of Nafion at a wide range of humidity. The proton conductivity of SBAF membranes with IEC = 1.5, 2.5 and 3.0 mequiv g^{-1} and Nafion membrane was 1.1, 10.6, 17.0, and 14.2 mS cm^{-1} at 30% RH, respectively. The proton conductivity of SBAF membranes was slightly higher than that of SPP-QP membranes, which was in agreement with the water uptake behaviour in Figure 37.

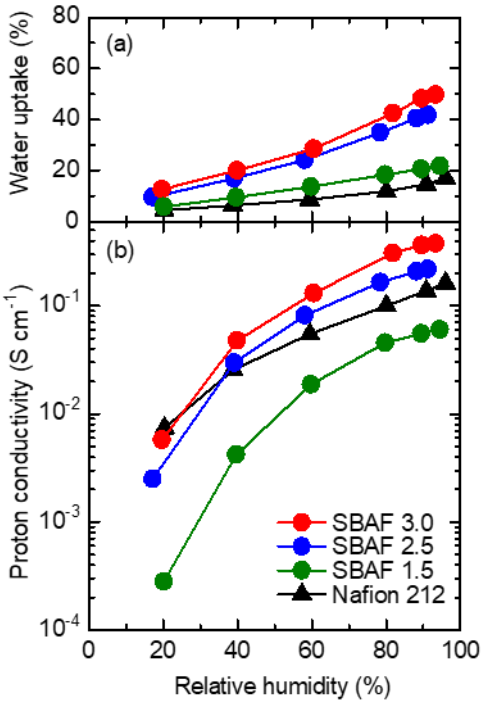

Figure 36. Humidity dependence of water uptake (a) and proton conductivity (b) of SBAF membranes at 80 ºC.

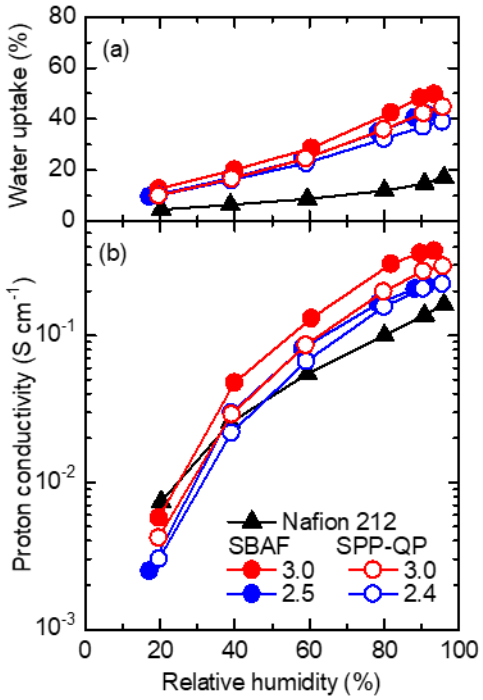

Figure 37. Humidity dependence of (a) water uptake and (b) proton conductivity of SBAF and SPP-QP membranes at 80 ºC.

The proton conductivity is re-plotted as a function of number of absorbed water molecules per sulfonic acid group (λ) in Figure 38. SBAF and SPP-QP membranes with comparable IEC values exhibited similar λ dependence of the conductivity, suggesting that the sulfonic acid groups and water molecules function similarly in these membranes. The proton diffusion coefficient (D_σ) was calculated from the Nernst-Einstein equation and is plotted as a function of volumetric IECv (which took absorbed water into account) in Figure 39. SBAF membranes exhibited higher diffusion coefficients than those of SPP-QP membranes. Taking into account the small phase-separated morphology and large water uptake, we postulate that the water molecules in the hydrophobic domains also contribute to the proton conduction in SBAF membranes. SBAF membrane with low IEC (= 1.5 mequiv g^{-1}), however, showed a significant dependence of the proton diffusion coefficient on the IECv due to the less connected ionic channels at low water content (or high IECv).

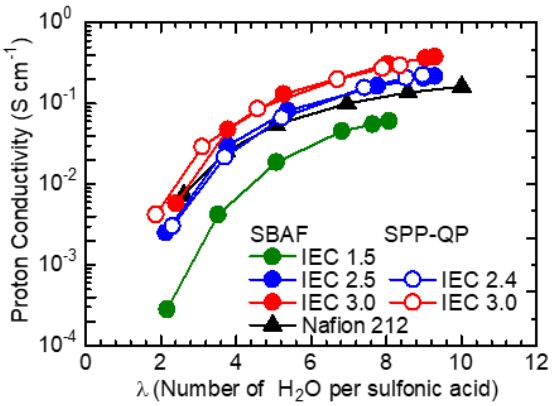

Figure 38. Proton conductivity as a function of number of absorbed water molecules per sulfonic acid group for SBAF, SPP-QP, and Nafion membranes at 80 ºC.

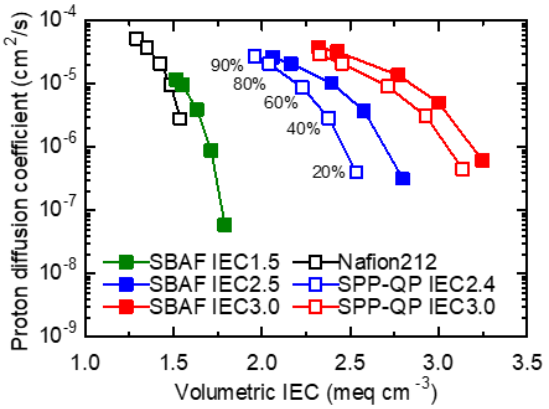

Figure 39. Proton diffusion coefficient of SBAF, SPP-QP and Nafion membranes as a function of volumetric IECv at 80 ºC.

3.3.4. Mechanical properties

Humidity dependence of storage modulus (E'), loss modulus (E''), and tan δ (= E''/E') of SBAF membranes was investigated by dynamic mechanical analyses (DMA) at 80 °C as shown in Figure 40. Three SBAF membranes with different IEC values showed similar viscoelastic properties with some losses in E' as increasing the humidity. The E'' and tan δ were stable with no obvious peaks suggesting these membranes did not have glass transition under the tested conditions. The E', E'', and tan δ curves of SBAF membranes were very similar to those of SPP-QP membranes with comparable IEC values (Figure 41), and thus the differences in the hydrophobic components did not affect the viscoelastic properties.

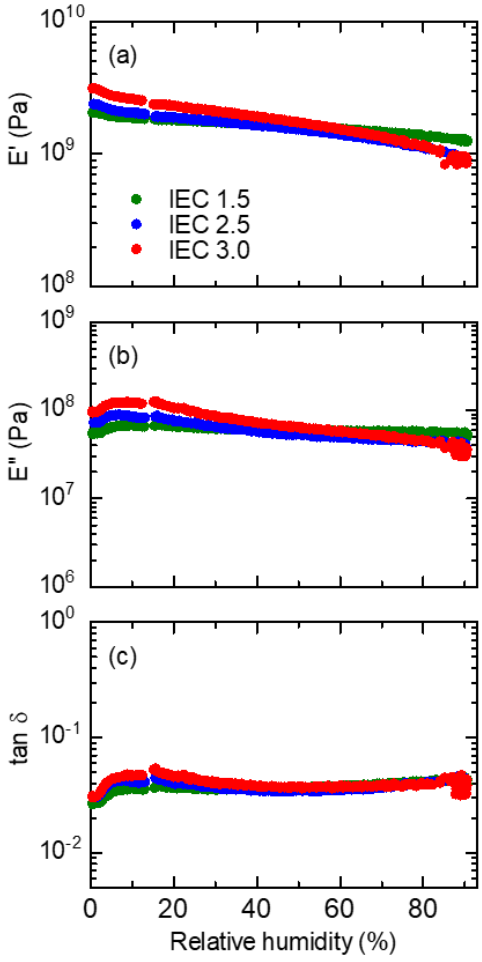

Figure 40. Dynamic mechanical analyses of SBAF membranes at 80 ºC as a function of the relative humidity.

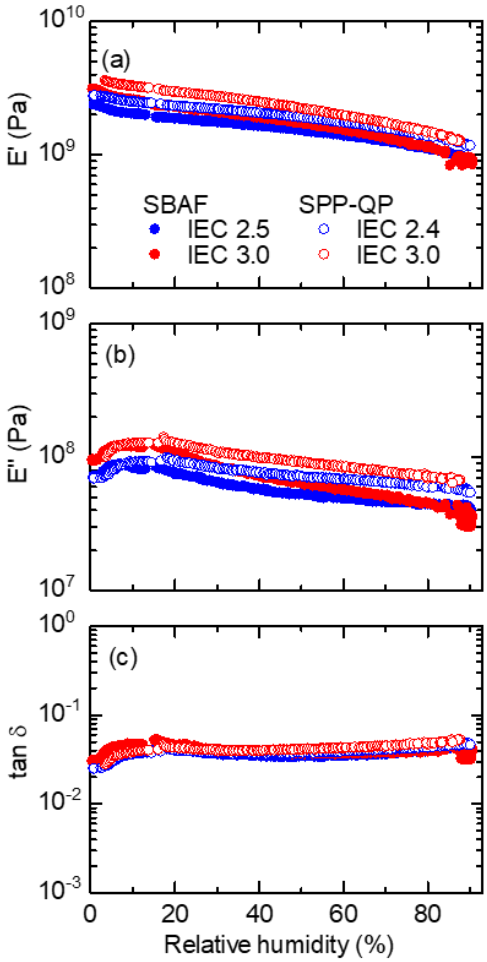

Figure 41. Dynamic mechanical properties of SBAF and SPP-QP membranes at 80 ºC as a function of the relative humidity.

Then, the elongation properties of SBAF membranes were examined at 80 °C and 60% RH, as shown in Figure 42 (stress/strain curves), and the results are summarized in Table 4. The SBAF membranes exhibited high Young's modulus (0.9-2 GPa) and maximum strength (33-79 MPa). Since the differences in their molecular weights were rather minor (Table 4), the elongation properties were more likely to be dependent on the IEC values. As shown in Figure 43, the lowest IEC (1.5 mequiv g^{-1}) SBAF membrane showed the highest maximum stress and maximum strain because the BAF groups as the hydrophobic component would be responsible for the mechanical strength. In addition, the lower IEC membrane absorbed less water. SBAF membranes showed similar elongation to those of SPP-QP membranes despite its less rigid hexafluoroisopropylidene groups than quinquephenylene groups.

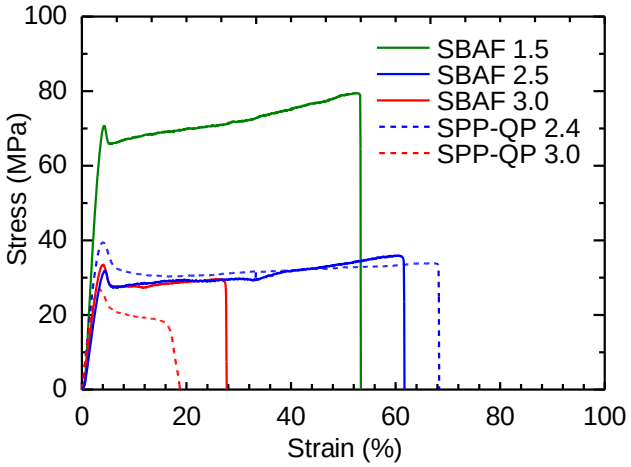

Figure 42. Stress versus strain curves of SBAF membranes at 80 ºC and 60% RH as reference SPP-QP membranes used.

Table 4. Summary of the tensile test results of SBAF membranes

No	Titrated IEC (mequiv g^{-1})	Maximum strain (%)	Young's modulus (GPa)	Maximum strength (MPa)
1	1.5	53	2	79
2	2.5	61	0.8	33
3	3.0	28	0.9	34

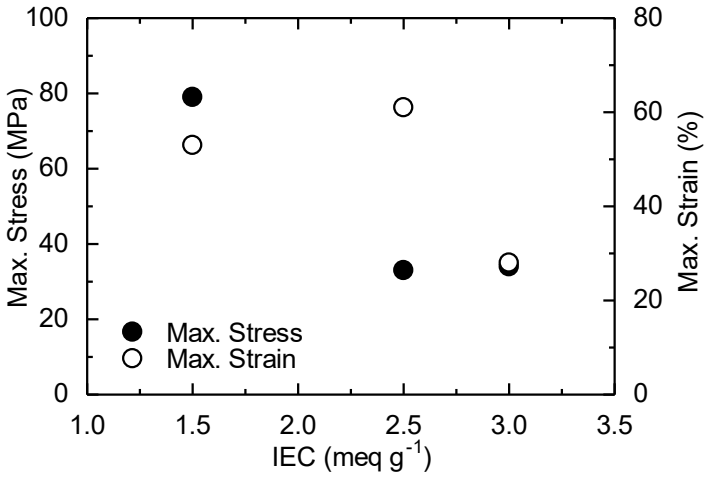

Figure 43. IEC dependence of maximum strength and maximum strain of SBAF membranes at 80 ºC and 60% RH.

3.3.5. Oxidative stability in Fenton's reagent

The oxidative stability of SBAF membranes was evaluated in Fenton's reagent at 80 °C for 1 h. The post-test SBAF membranes retained flexibility with no cracks and brittleness unlike typical aromatic hydrocarbon ionomer membranes. The remaining weights and IECs were both 100% (Table 5). The molecular weights decreased only slightly with 92 - 99% remaining (Figure 44). ^{1}H and ^{19}F NMR spectra and the copolymer compositions obtained therefrom did not change after the Fenton's test (Figure 45). Water uptake, proton conductivity, and their humidity dependence were measured at 80 °C for the post-test membranes and compared to those of the pristine membranes. As shown in Figure 46, post-test and pristine membranes exhibited very similar properties within acceptable errors. Furthermore, viscoelastic properties of the membranes did not change after the oxidative stability test (Figure 47). However, the post-test membranes showed smaller strains in stress versus strain curves (Figure 48) than those of the pristine membranes. The loss in mechanical properties might be related with minor losses in molecular weights and/or morphological changes during the Fenton's test. The high oxidative stability of SBAF membranes was similar to SPP-QP membranes, suggesting hexafluoroisopropylidene groups did not experience oxidation reaction by peroxide radicals.

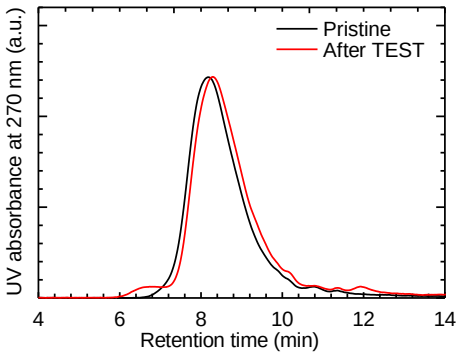

Figure 44. GPC profiles of SBAF membrane (IEC = 3.0 mequiv g^{-1}) before (black) and after (red) the Fenton's test.

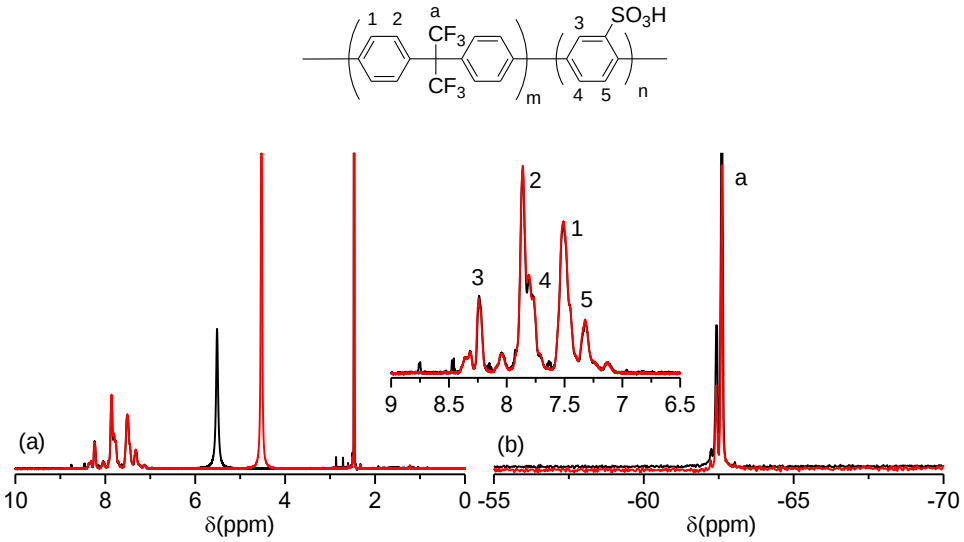

Figure 45. (a)^{1}H and (b) ^{19}F NMR spectra of SBAF membrane (IEC = 3.0 mequiv g^{-1}) before (black) and after (red) the Fenton's test.

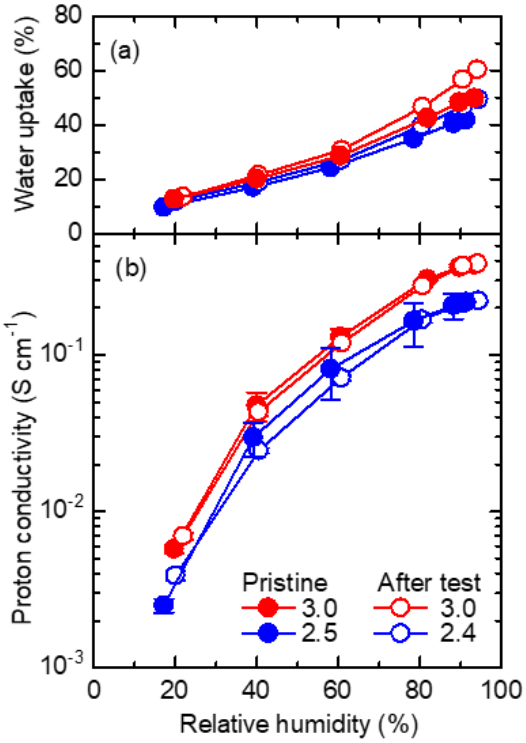

Figure 46. Humidity dependence of (a) water uptake and (b) proton conductivity of SBAF membranes at 80 ºC before and after the Fenton's test.

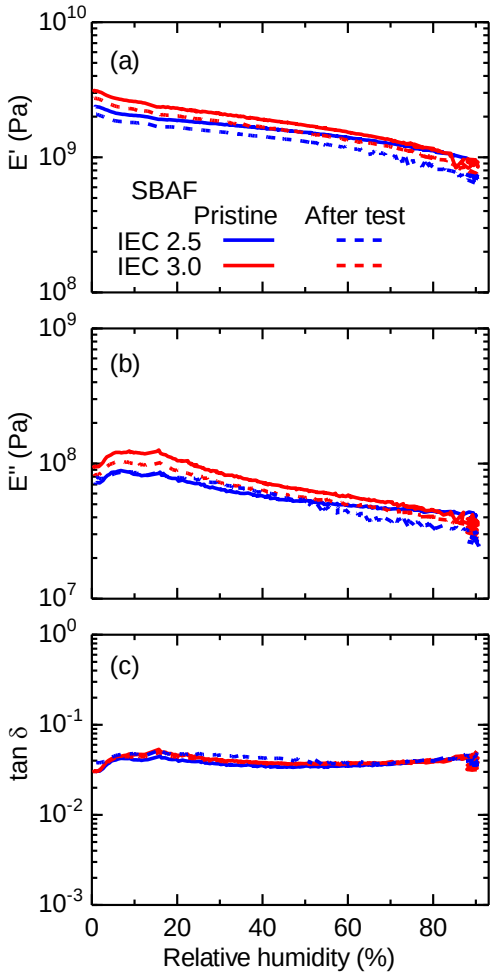

Figure 47. Dynamic mechanical properties of SBAF membranes at 80 ºC before (solid) and after (dashed) the Fenton's test.

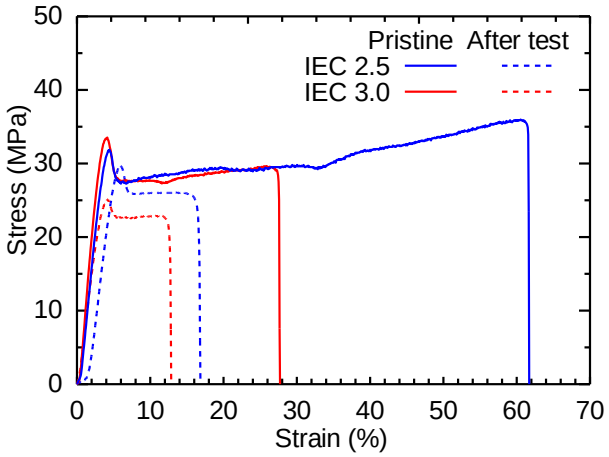

Figure 48. Stress versus strain curves of SBAF membranes at 80ºC and 60% RH before (solid) and after (dashed) the Fenton's test.

3.3.6. Gas permeability

The gas permeability of SBAF membranes was measured at 80 °C as a function of RH (Figure 49) and compared with those of Nafion NRE212 and SPP-QP (IEC = 2.4 mequiv g^{-1}) membranes. SBAF membrane (IEC = 2.6 mequiv. g^{-1}; please note that SBAF 2.5 was re-synthesized for the gas permeability and fuel cell experiments and the obtained polymer had a slightly higher IEC) exhibited significantly lower hydrogen and oxygen permeability than that of Nafion membrane from 30% to 90% RH. The lower gas permeability is intrinsic for aromatic ionomer membranes. The permeability of SBAF membrane was higher than that of SPP-QP membrane. The quinquephenylene moieties as hydrophobic groups could have closer intermolecular packing among the polymer chains to cause lower gas permeability. Unlike the other two membranes, the gas permeability of SBAF membrane decreased as increasing the humidity presumably related with its higher water absorbability since gases are more likely to permeate through the hydrophobic domains than the hydrophilic domains in ionomer membranes.

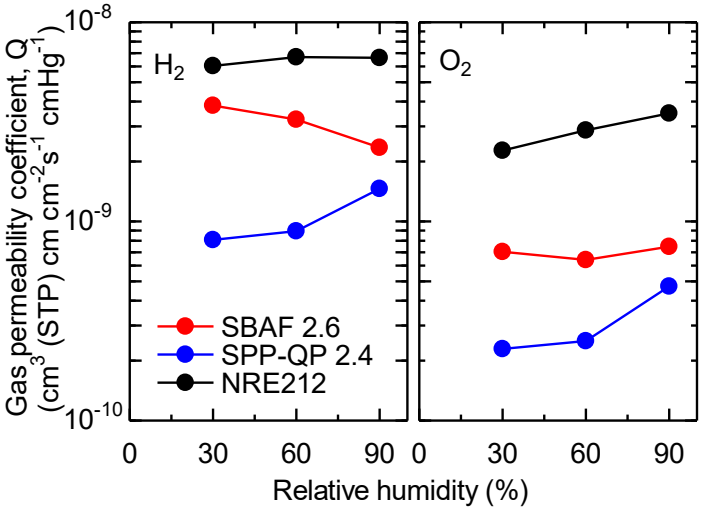

Figure 49. Hydrogen and oxygen permeability at 80 ºC as function of relative humidity.

3.3.7. Fuel cell performance

Because of the balanced properties of water uptake, proton conductivity, mechanical properties, and their humidity dependence, SBAF 2.5 (IEC = 2.6 mequiv g^{-1}) was chosen for fuel cell evaluation. A catalyst-coated membrane (CCM) was prepared from the SBAF membrane (30 μm thick) with catalyst layers consisting of Pt/CB catalyst and Nafion binder for both the anode and the cathode. Figure 50 shows polarization curves and ohmic resistances under humidity conditions of 100% RH and 30% RH. The open circuit voltage (OCV) was reasonably high, 1.02 V (oxygen, 100% RH), 1.02 V (air, 100% RH), 1.03 V (oxygen, 30% RH), and 1.00 V (air, 30% RH), reflecting low gas permeability of the SBAF membrane. At 100% RH, ohmic resistance of the SBAF cell was as low as 0.05 Ω cm^2 both with oxygen and air, which was comparable to that (0.03 Ω cm^2) calculated from the proton conductivity and thickness of the membrane. At 30% RH, the ohmic resistance was ca. 0.3 Ω cm^2 at OCV, which was also similar to the calculated one (0.28 Ω cm^2) from the proton conductivity and thickness. The ohmic resistance decreased as increasing the current density at 30% RH because of the back-diffusion of water from the cathode into the membrane. The effect was more pronounced with oxygen than with air since the gas flow rate was slower for oxygen under the constant gas utilization conditions. The SBAF cell exhibited better fuel cell performance than the SPP-QP and Nafion cells at 30% RH. The SBAF cell owed high fuel cell performance partly to the low ohmic resistance. Since the proton conductivity of SBAF membrane was not higher than those of SPP-QP and Nafion membranes, the low ohmic resistance would imply good interfacial compatibility of the membrane with the catalyst layers. In the IR-corrected polarization curves (Figure 51), the SBAF cell exhibited the best performance while these three cells utilized the same Nafion-based catalyst layers. The high electrode (cathode) performance with the SBAF membrane also supported good interfacial compatibility.

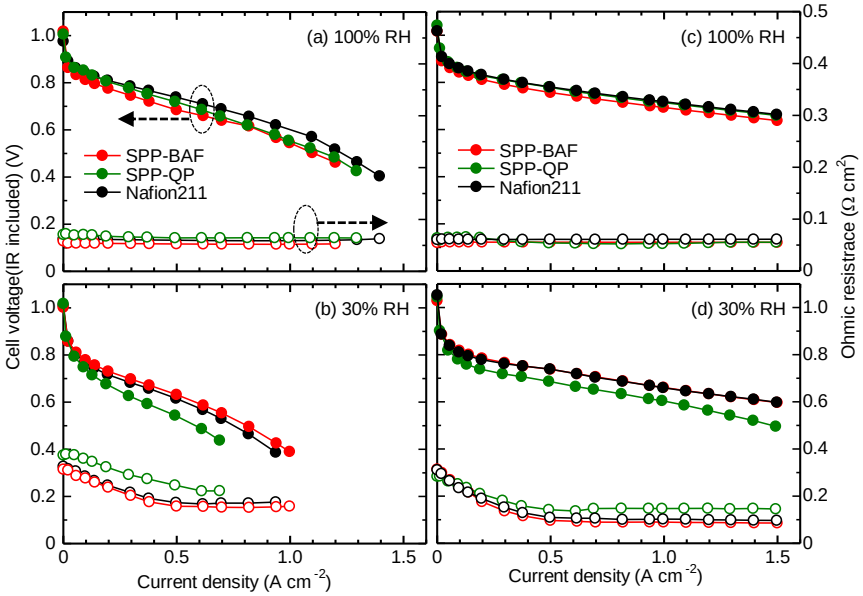

Figure 50. IR-included polarization curves and ohmic resistances of a fuel cell with SBAF membrane (IEC = 2.6 mequiv g^{-1}) at 80 ºC, (a) 100% and (b) 30%RH with air, and (c) 100% and (d) 30% RH with O_2.

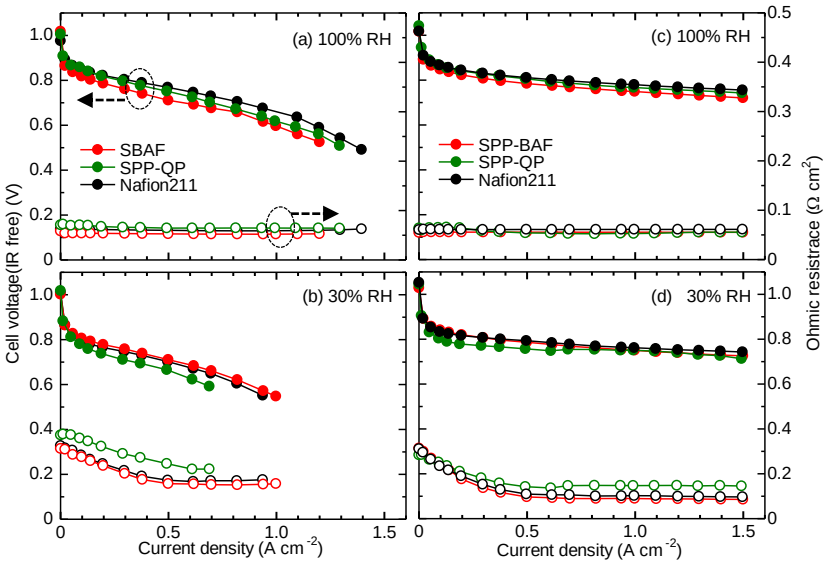

Figure 51. IR-free polarization curves and ohmic resistances of a fuel cell with SBAF membrane (IEC = 2.6 mequiv g^{-1}); (a) 100% and (b) 30% RH with air, and (c) 100% and (d) 30% RH with O_2 at 80 ºC.

To evaluate the durability of SBAF membrane, OCV hold test was carried out at 80 °C and 30% RH with hydrogen and air (Figure 52). The initial OCV was 1.00 V and decreased only slightly to 0.97 V after 1000 h with the average decay of -40 μV h^{-1}. SBAF membrane exhibited much better chemical durability than SPP-QP membrane, which showed 1.00 V of the initial OCV and 0.80 V of the post-mortem OCV with -226 μV $h^{-1}$of the average decay. After the OCV hold test, the IV performance was re-evaluated under the same conditions as shown in Figure 53. The changes in OCVs were very minor, from 1.02 to 1.01 V (oxygen, 100% RH), 1.02 to 1.01 V (air, 100% RH), 1.03 to 1.02 V (oxygen, 30% RH), and 1.00 to 0.99 V (air, 30% RH), respectively. The post-mortem cell exhibited comparable performance at 100% RH and lower performance at 30% RH compared to those of the pristine cell. The lower performance at 30% RH was caused somewhat higher ohmic resistance. Then, the fuel cell was disassembled and the post-mortem SBAF membrane was recovered by removing carefully the catalyst layers from both sides of the membrane. The recovered membrane retained transparency and flexibility. ^{1}H and ^{19}F NMR spectra as well as the GPC measurement did not show detectable evidences of the chemical degradation in the post-mortem SBAF membrane (Figure 54). Therefore, the increased ohmic resistance of the post-mortem cell at 30% RH was due likely to the interfacial incompatibility with the catalyst layers, but not the membrane degradation.

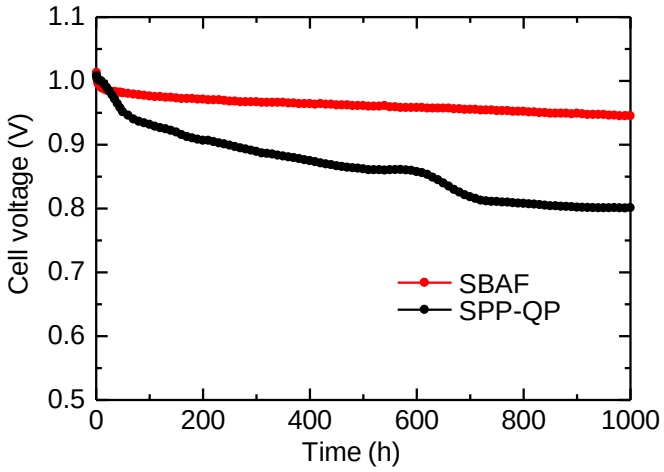

Figure 52. OCV hold test of SBAF (IEC = 2.6 mequiv g^{-1}) and SPP-QP (IEC = 2.4 mequiv g^{-1}) cells at 80 ºC and 30% RH.

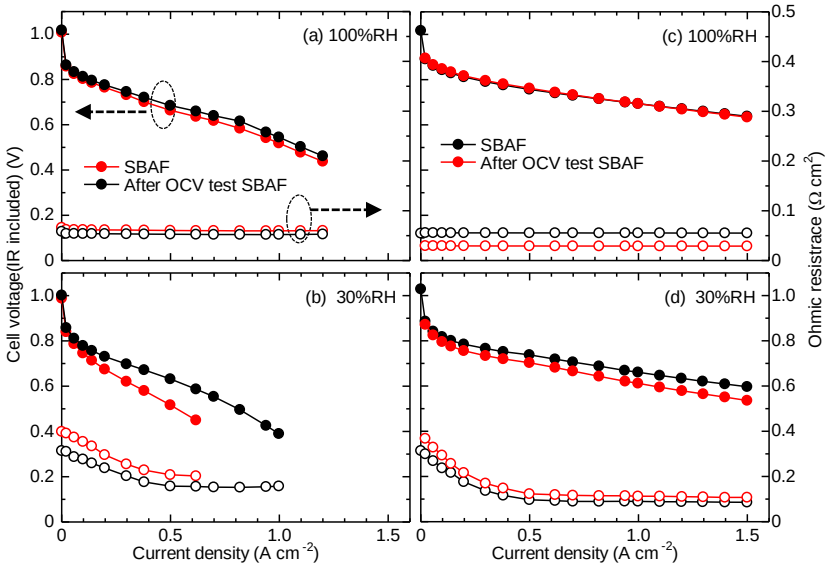

Figure 53. IR-included polarization curves and ohmic resistances of a fuel cell with SBAF membrane (IEC = 2.6 mequiv g^{-1}) at 80 °C, (a) 100% and (b) 30% RH with air, and (c) 100% and (d) 30% RH with O_2 after the OCV hold test.

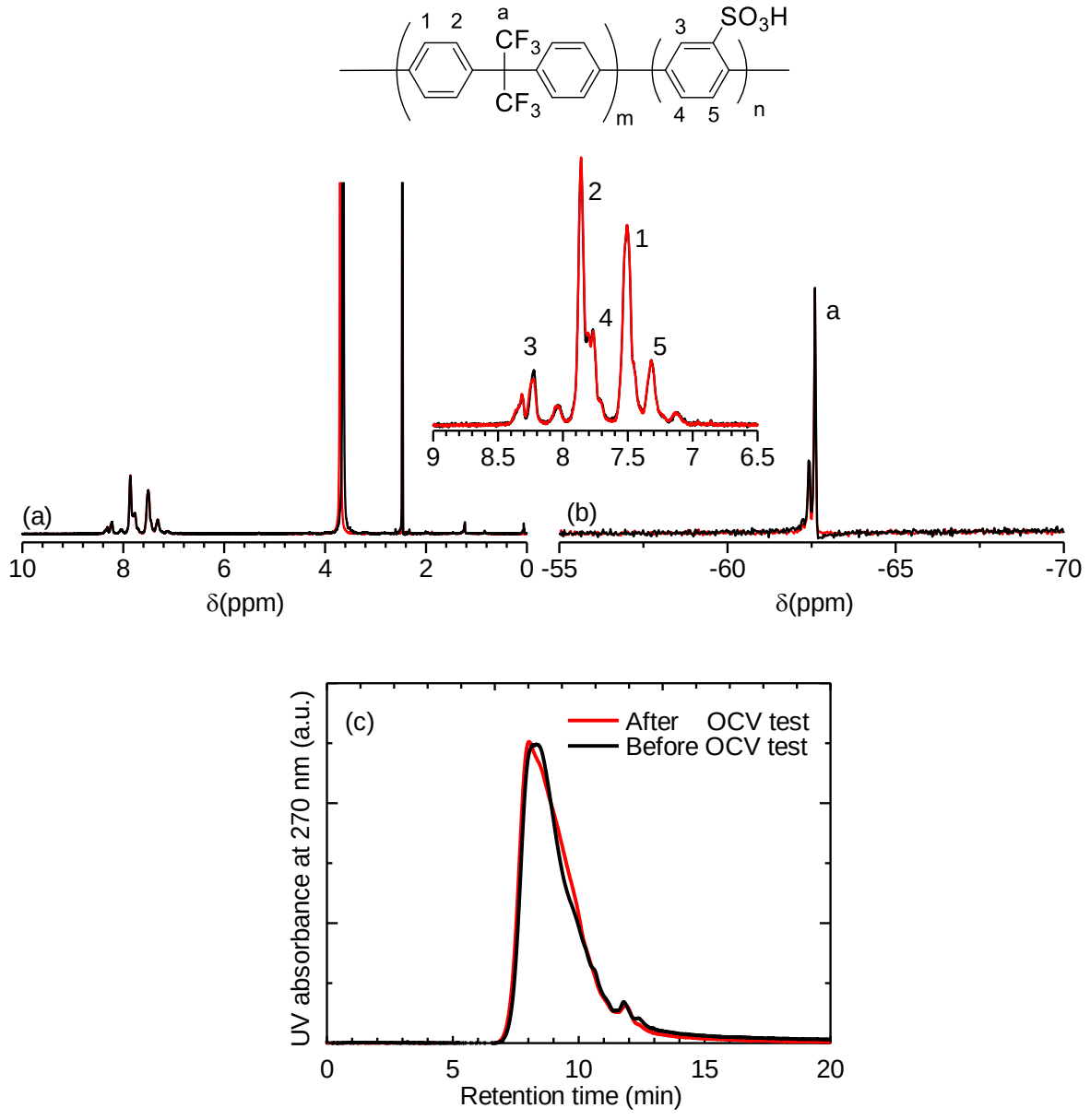

Figure 54. (a) ^{1}H and (b) ^{19}F NMR spectra, and (c) GPC profiles of SBAF membrane (IEC = 2.6 mequiv g^{-1}) before (black) and after (red) the OCV hold test.

3.4. Conclusions

A series of novel sulfonated aromatic polymers (SBAF) containing sulfophenylene (SP) and hexafluoroisopropylidene biphenylene (BAF) groups were successfully synthesized by Ni(0)-promoted coupling reaction. BAF groups as hydrophobic component provided the resulting sulfonated polyphenylenes with good membrane forming capability. Compared to our previous sulfonated polyphenylene (SPP-QP) membranes, the newly prepared SBAF membranes exhibited higher water absorbability, higher proton conductivity, similar mechanical and chemical stabilities, and higher hydrogen and oxygen gas permeability. The higher proton conductivity was the result of higher proton diffusion coefficient. In hydrogen/air (or oxygen) fuel cell, SBAF membrane exhibited better performance The higher gas permeability of SBAF membrane caused slightly lower initial OCV (1.02 V) than that of SPP-QP (1.05 V). Nevertheless, SBAF membrane was durable in OCV hold test for 1000 h with a small decay in OCV value (-40 $\mu V\ h^{-1}$). The post-mortem membrane (after the OCV hold test) showed minor changes in the chemical structure and molecular weight. However, since the mechanical stability was deteriorated in the ex-situ accelerated chemical stability test (Fenton's test), interfacial incompatibility must have occurred during the OCV hold test to cause the performance loss in the fuel cell at low humidity.

References

[1] J. Miyake, R. Taki, T. Mochizuki, R. Shimizu, R. Akiyama, M. Uchida and K. Miyatake, *Sci. Adv.*, 2017, 3, eaao0476

[2] P. A. Havelka-Rivard, K. Nagai, B. D. Freeman, and V. V. Sheares, *Macromolecules*, 1999, 32, 6418–6424.

Chapter 4. The simple design of novel partially fluorinated polymers containing trifluoromethyl (-CF_3-) group on sulfonated polyphenylene

4.1. Introduction

Many researchers have considered to develop partially-fluorinated sulfonated aromatic materials. [1-4] Not only according to the literature but also according to the results in Chapters 2 and 3, fluorinated groups have been proven to possess attractive and helpful effects, although non-fluorinated membranes have been required for environment compatibility. The strong carbon-fluorine bond in the membranes can support high chemical stability and durability under harsh conditions and enhanced mechanical stability due to the flexible bond. As seen in the results in Chapter 3, the SBAF membranes have high proton conductivity and superior durability during an OCV hold test for 1000 hours. However, the higher gas permeability of SBAF could potentially be deleterious in long-term fuel cell operation, due to the hexafluoroisopropylidene group on the main chain. Novel partially fluorinated polymers (STF) were suggested to be desirable to decrease the gas permeability and robust membranes under humid conditions. Combinations of STF polymers as homo-, co- and ter-polymers with various commercially available dichlorobenzotrifluoride (TF) monomers and sulfonated benzene (SP) were considered and their membrane properties determined. The flexible hexafluoroisopropylidene group on SBAF was replaced with phenyl-bonds and trifluoro-methyl groups on the benzene ring. All STF polymers were prepared by the Ni(0)-catalyst coupling reaction. By comparing with the SBAF membrane, trifluoro-methyl groups effects were investigated.

4.2. Experimental

4.2.1. Measurements

^{1}H and ^{19}F NMR spectra were measured with a JEOL JNM-ECA/ECX500 using deuterated chloroform ($CDCl_3$) or dimethyl sulfoxide (DMSO-d_6) with tetramethylsilane as an internal reference. The molecular weight was measured via gel permeation chromatography (GPC) equipped with a Jasco 805 UV detector. Dimethylformamide (DMF) containing 0.01 M lithium bromide (LiBr) was used as eluent. Shodex KF-805L column was used for the measurement of polymers and monomers.

Molecular weight was calibrated using standard polystyrene samples.

Ion exchange capacity (IEC) of the membranes was measured by titration at r.t. A piece of dry membrane in acid form was immersed into 2 M NaCl aqueous solution for at least 24 h. The solution was titrated with 0.1 M NaOH aqueous solution. The IEC was calculated using the following equation; IEC (mequiv. g^{-1}) = $\Delta V_{NaOH} \times C_{NaOH} / W_d$, where W_d is weight of dry membrane, ΔV_{NaOH} is consumed volume of the NaOH solution, and C_{NaOH} is the concentration of the NaOH solution.

The proton conductivity and water uptake were measured with a solid electrolyte analyzer system (MSBAD-V-FC, Bel Japan Co.) equipped with a temperature and humidity controllable chamber. The weight of the membranes at a given humidity was measured by magnetic suspension balance. The water uptake was calculated by the following equation. Water uptake = (weight of hydrated membrane) – (weight of dry membrane) / weight of dry membrane × 100. The membranes were dried at 80 ºC for 3 h under vacuum to obtain the weight of dry membranes and exposed to the set humidity for at least 2 h to obtain the weight of hydrated membranes. In-plane proton conductivity (σ) of the membranes was measured by ac impedance spectroscopy (Solartron 1255B and 1287) simultaneously in the same chamber. Ion conducting resistances (R) were determined from the impedance plot measured over the frequency range from 1 to 10^5 Hz. The proton conductivity was calculated according to the following equation; $\sigma = L / (S \times R)$, where L and S are the distance of the electrodes and the cross-sectional area of the membrane, respectively.

Dynamic mechanical analyses (DMA) of the membranes (5 mm × 30 mm) were carried out by an ITK DVA-225 dynamic viscoelastic analyzer at 80 ºC from 0 to 90% RH at 10 Hz. The storage moduli (E'), loss moduli (E''), and tan σ (= E''/E') of the membranes were measured. Tensile strength of the membranes was measured with a Shimadzu AGS-J 500N universal test machine attached with a Toshin Kogyo Bethel-3A temperature and humidity controllable chamber at 80 ºC and 60% RH at a stretching rate of 10 mm min^{-1}. Stress versus strain curves were obtained for samples cut into a dumbbell shape (DIN-53503-S3, 35 mm × 6 mm (total) and 12 mm × 2 mm (test area)).

4.2.2. Materials

3,4-, 2,5-, and 2,4-dichlorobenzotrifluoride (TCI), 2,2'-Bis(trifluoromethyl)benzidine (TCI), 2,5-dichlorobenzenesulfonic acid dehydrate (SP) (TCI), bis(1,5-cyclooctadiene)nickel(0) ($Ni(COD)_2$) (> 95%, Kanto Chemical), 2,2'-bipyridine (> 99%, Kanto Chemical), Copper (I) chloride (> 99%, Kanto Chemical), Sodium nitrite(Kanto Chemical), potassium carbonate (K_2CO_3) (Kanto Chemical),

sodium chloride (NaCl) (Kanto Chemical), dimethyl sulfoxide (DMSO) (> 99%, Kanto Chemical), and toluene (> 99%, Kanto Chemical) were used as received.

4.2.3. Synthesis of homo-, co- and ter-polymers with dichlorobenzotrifluoride

A typical procedure for STF-ter-1 is as follows. A 100 mL three-neck flask was charged with 3,4-dichlorobenzotrifluoride (0.3 g, 1.4 mmol), 2,5-dichlorobenzotrifluoride (0.3 g, 1.4 mmol), SP (0.1842 g, 0.7 mmol), K_2CO_3 (0.1161 g, 0.84 mmol), 2,2'-bipyridine (09196 g, 5.860 mmol), dimethyl sulfoxide (DMSO, 6 mL), and toluene (6 mL). The mixture was heated at 170 ºC for 2 h with a Dean Stark trap under N_2. After azeotropic dehydration, the mixture was cooled to 80 ºC. To the mixture, $Ni(COD)_2$ (1.6120g, 5.860 mmol) was added. After the reaction at 80 ºC for 3 h, the mixture was poured into large excess of 6 M HCl to precipitate the product. The crude product was washed with concentrated HCl and deionized water several times. The targeted terpolymer was obtained by drying at 80 ºC in a vacuum oven overnight in 43-67% yield.

4.2.4. Synthesis of 4,4'-dichloro-2,2'-bis(trifluoromethyl)biphenyl

4,4'-dichloro-2,2'-bis(trifluoromethyl)biphenyl was designed and synthesized by Sand-meyer reaction as follow; A one neck flask was charged with 2,2'-bis(trifluoromethyl) benzidine (2g, 6.24mmol) and 5M HCl(25ml). After all powder was dissolved mixed, solution [A+B] was dropping in one neck flask and stirred for 24hours. Prepared solution A [$NaNO_2$(1.04g, 14.98mmol) dissolved in DIW(3.31ml)] was dropping slowly in solution B [CuCl(2.22g, 22.47mnol) dissolved in 12M HCl(17ml)]. The solution was added ethyl acetate and did extraction, collected organic layer, washed with 0.1M HCl several time, washed with DIW several time, collected organic layer. Evaporated solvent then short column with Aluminum Oxide and eluent solvent; Hexane. White crystal powder was prepared and yield of that is 42%, 0.9g.

4.2.5. Co-polymerization (STF-BP) with 4,4'-dichloro-2,2'-bis(trifluoromethyl)biphenyl

A typical procedure for STF-BP is as follows. A 100 mL three-neck flask was charged with 4,4'-dichloro-2,2'-bis(trifluoromethyl)biphenyl (0.5 g, 1.4 mmol), SP (0.3157 g, 1.2 mmol), K_2CO_3 (0.1990 g, 1.44 mmol), 2,2'-bipyridine (1.7084 g, 10.8 mmol), dimethyl sulfoxide (DMSO, 8 mL), and toluene (8 mL). The mixture was heated at 170 ºC for 2 h with a Dean Stark trap under N_2. After

azeotropic dehydration, the mixture was cooled to 80 ºC. To the mixture, $Ni(COD)_2$ (1.4974g, 5.4 mmol) was added. After the reaction at 80 ºC for 3 h, the mixture was poured into large excess of 6 M HCl to precipitate the product. The crude product was washed with concentrated HCl and deionized water several times. The targeted terpolymer was obtained by drying at 80 ºC in a vacuum oven overnight in > 97% yield.

4.2.6. Membrane preparation

A STF-BP copolymer in sodium ion form was dissolved in DMSO (5-10% w/v). The solution was cast onto a clean glass plate and dried at 80 ºC for 1 d. The resulting membranes (ca. 50 μm thick) were converted to acid form with 1 M H_2SO_4 for 1 d at room temperature, washed with deionized water several times, and dried at r.t.

4.3. Results and discussion

4.3.1. Synthesis of STF polymer as homo-, co- and ter-polymers

A series of homo-, co- and ter-polymer with dichlorobenzotrifluoride and sulfophenylene (SP) was prepared by ni(0)-catalyst coupling reaction as follow Scheme 3. The 3 different dichlorobenzotrifluoride monomers, 3,4- (1), 2,5- (2) and 2,4- dichlorobenzotrifluoride (3), were controlled to determine possibility to obtain polymer with high molecular weight as summarized in Table 5. However, all combination did offer low molecular weight (Mw < 20kDa) then it could not give flexible membranes. As shown in Figure 55, determined ^1H NMR spectrum of STF-ter-polymers could not be well-assigned due to overlap of aromatic peaks. However, ^{19}F NMR spectrum of that explained unsuccessful polymerization because of appeared peaks at -61 ~ -63 ppm of characteristic peak for not polymerized dichlorobenzotrifluoride.

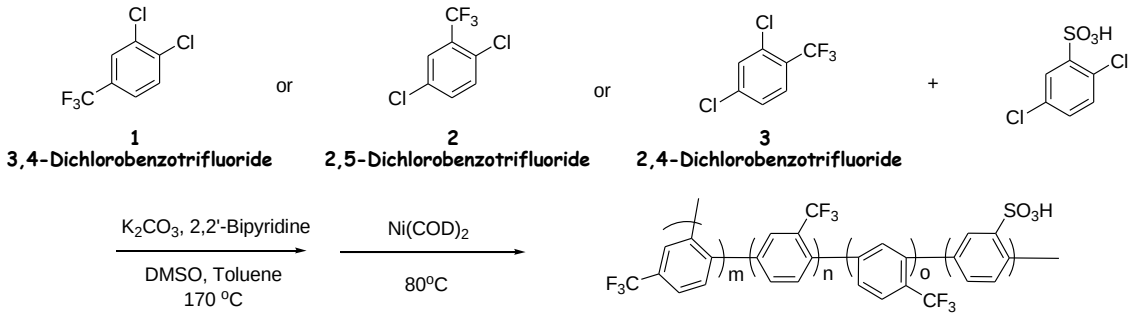

Scheme 3. Polymerization of *homo-, co-,* and *ter*-polymers between dichlorobenzotrifluoride and sulfophenylene (SP).

Table 5. Summary of synthesis feed ratio, molecular weight and yield of polymerization.

	m : n : o	SP	Molecular Weight (kDa)			Yield
	(m mol)	(m mol)	Mn	Mw	PDI	(%)
Homo-1	0.6 : 0 : 0	0	0.4	1	2.87	x
Homo-2	0 : 0.6 : 0		4	8	1.9	96
Homo-3	0 : 0 : 0.6		4	7	1.64	96
Co-1	0.6 : 0 : 0	0.7	3.7	6	1.84	50
Co-2	0 : 0.6 : 0		5	12	2.59	38
Co-3	0 : 0 : 0.6		4	20	2.43	57
Ter-1	0.3 : 0.3 : 0		4	11	2.63	43
Ter-2	0.3 : 0 : 0.3		3.7	10	2.58	57
Ter-3	0 : 0.3 : 0.3		3.7	10	1.65	67

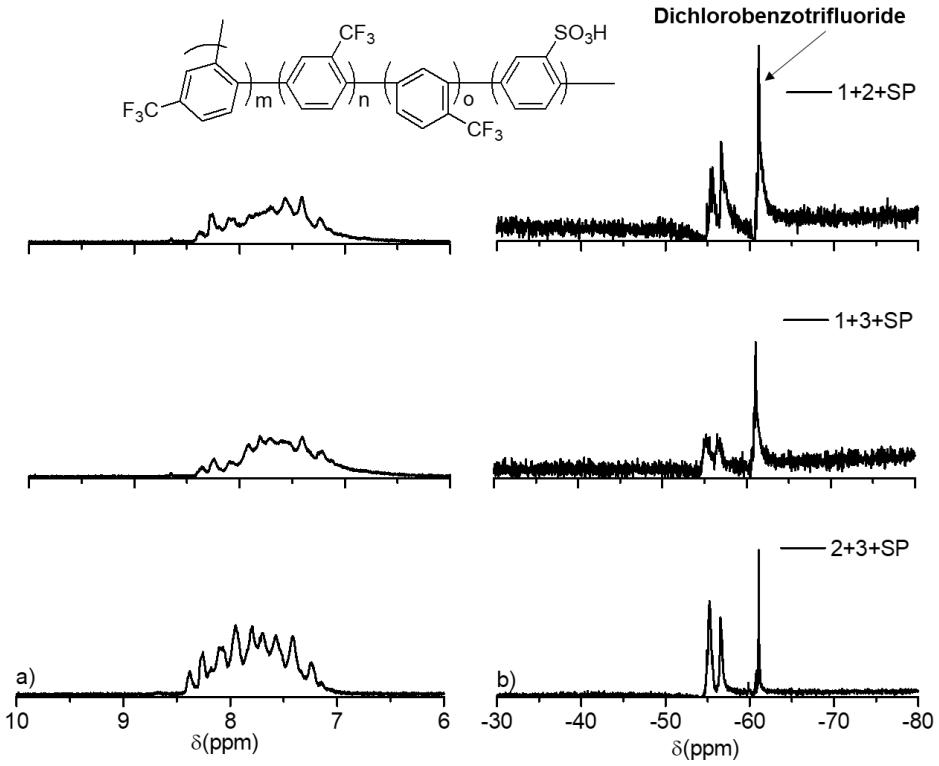

Figure 55. (a)^{1}H and (b) ^{19}F NMR spectrum of STF-ter-polymers in DMSO-$_{d6}$ at 80°C.

4.3.2. Co-polymerization with synthesized 4,4'-dichloro-2,2'-bis(trifluoromethyl)biphenyl (STF-BP)

A series of STF-BP copolymers was suggested to improve molecular weight to form membranes, because the prepared polymers with mono-dichlorobenzotrifluoride have insufficient molecular weight. The BP type of dichlorobenzotrifluoride, 4,4'-dichloro-2,2'-bis(trifluoromethyl)biphenyl, was synthesized successfully by Sand Meyer reaction, > 50% of yield, as shown in Scheme 4 (red-route) and obtained monomer was measured and well-assigned by NMR, as shown in Figure 56-(2). The STF-BP copolymers were polymerized by Ni(0)-promoted coupling reaction with high molecular weight (Mw > 118kDa), as explained in Scheme 4 (blue-route) and high yield (> 96%), as summarized in Table 6 and measured by NMR as shown in Figure 56-(3) and well-assigned to the supposed chemical structure. The IEC values of STF-BP copolymer were controlled by feed ratio of SP monomers; the expected IEC values were 1.7 and 3.0 mequiv g^{-1}, which were determined by titration to be 1.5 and 2.5 mequiv g^{-1} respectively. Both copolymers provided flexible and transparent membranes. The higher IEC values of STF-BP copolymer were difficult to prepare due to the rigid backbone based on para-para phenyl combination. Perhaps the design of meta-para combination (4/1) could help to achieve membrane formation.

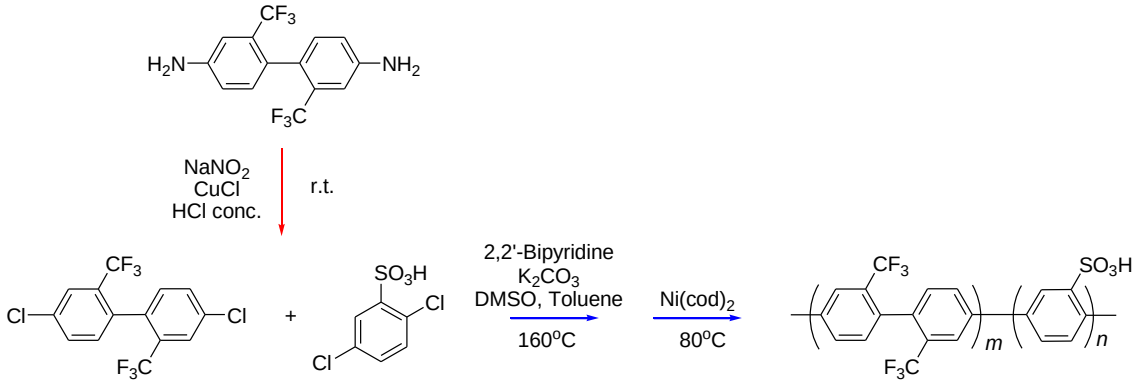

Scheme 4. (red) Synthesis of 4,4'-dichloro-2,2'-bis(trifluoromethyl)biphenyl and (blue) Polymerization of STF-BP copolymers.

Table 6. Composition, molecular weight, and ion exchange (IEC) of STF-BP copolymer.

	m : n	Molecular Weight (kDa)[a]			IEC (mequiv g^{-1})		Yield
	(m mol)	Mn	Mw	PDI	Targeted[b]	Titrated[c]	(%)
1	1.39 : 1.2	71	179	2.52	1.7	1.5	97
2	1.39 : 2.6	23	118	1.9	3.0	2.5	97

[a] Determined by GPC (DMF containing 0.01 M LiBr was used as eluent). [b] Calculated from the feed monomer compositions assuming 100% conversion. [c] Obtained from titration.

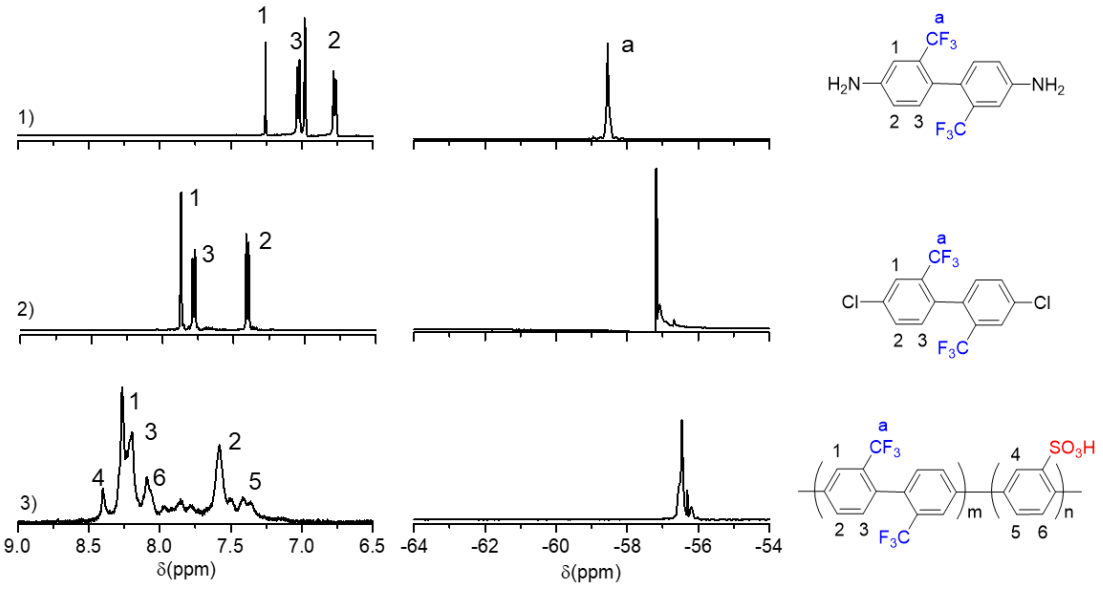

Figure 56. eft)^{1}H and (right) ^{19}F NMR spectrum of 1) 2,2'-bis(trifluoromethyl) benzidine in $CDCl_3$ at r.t. 2) synthesized 4,4'-dichloro-2,2'-bis(trifluoromethyl)bipheyl in DMSO-$_{d6}$ at 80°C and 3) obtained copolymer in DMSO-$_{d6}$ at 80°C, respectively.

4.3.3. Proton conductivity and Water uptake

Figure 57 shows proton conductivity and water uptake of STF-BP membranes at 80 ºC as a function of relative humidity (RH). For reference, data for SBAF membrane is also included. Water uptake and proton conductivity increased with increasing IEC for the STF-BP membranes. The water uptake of STF-BP membranes with similar IECs was higher than those of SBAF membrane at a wide range of humidity with different hydrophobic component. However, in proton conductivity, STF-BP membrane with low IEC (1.5 mequiv g^{-1}) exhibited similar proton conductivity with SBAF value membrane under > 40%RH condition. Interestingly, the proton conductivity of STF-BP membrane under lower humidity condition, < 40%RH condition, is significantly higher than those of SBAF. In higher IEC (2.5 mequiv g^{-1}), STF-BP membrane have higher water uptake and higher proton conductivity. Basically, the chemical structure of both membranes is similar, and thus, the different water affinity might be related to the location of the trifluoromethyl (CF_3) groups on the backbone. According to that, various positions and compositions of polymers need to be investigated.

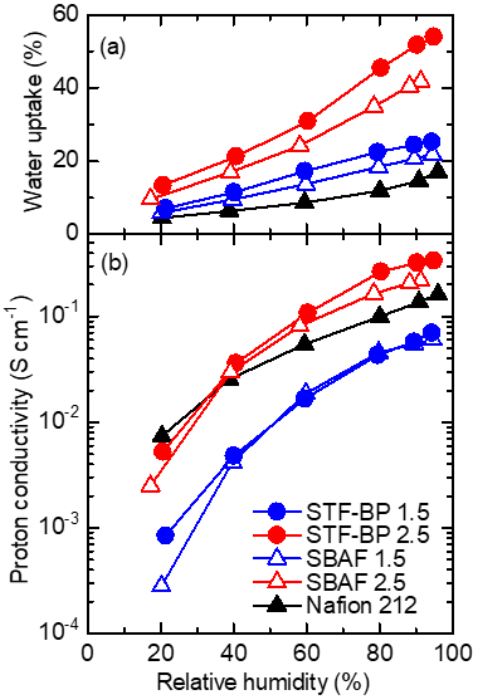

Figure 57. Humidity dependence of (a) water uptake and (b) proton conductivity of STF-BP copolymer and SBAF as reference at 80ºC.

4.3.4. Mechanical properties

Humidity dependence of the storage modulus (E'), the loss modulus (E''), and tan δ (= E''/E') of the STF-BP membranes (IEC 1.5 mequiv g^{-1}) was investigated by dynamic mechanical analysis (DMA) at 80 ºC, as shown in Figure 58 and compared with SBAF membrane (IEC 1.5 mequiv g^{-1}). Both membranes exhibited similar viscoelastic properties without obvious transition behavior under humidity conditions. STF-BP membrane showed higher in E' and E'' at entire humidity test condition compared to those of SBAF membranes due to rigid structure of backbone, para-para phenyl component. Figure 59 shows tensile test results (stress/strain curves) of STF-BP membranes at 80 ºC and 60% RH. The STF-BP membrane exhibited much less elongation properties than those of SBAF membrane, less than 10% of strain under humidity condition. The results are in agreement with the DMA data.

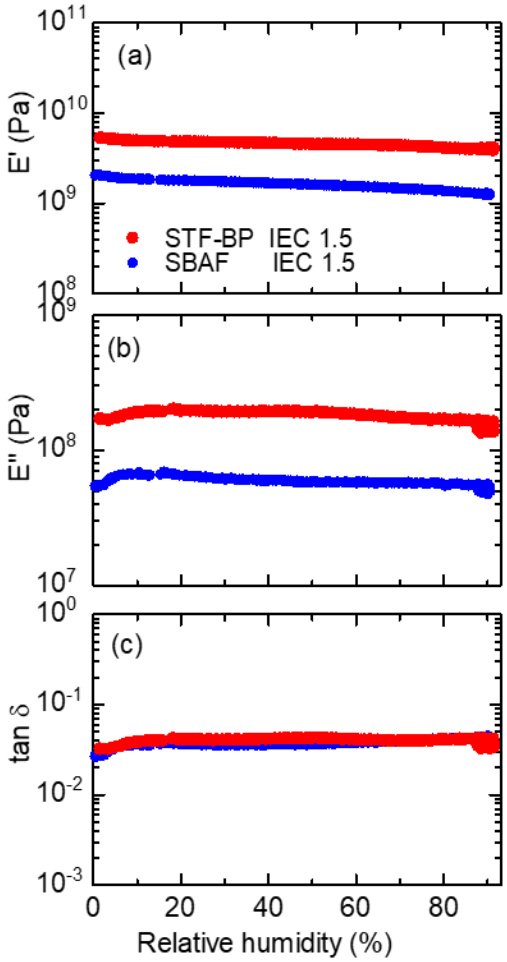

Figure 58. Dynamic mechanical analysis of new copolymer (IEC 1.7 mequiv g^{-1}) and SBAF (IEC 1.5 mequiv g^{-1}) as a function of the relative humidity: (a) E', (b) E'' and (c) tan σ, respectively.

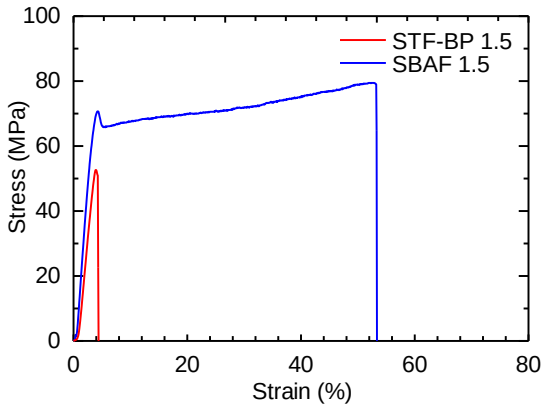

Figure 59. Stress versus strain curve of new copolymer (IEC 1.7 mequiv g^{-1}) and SBAF (IEC 1.5 mequiv g^{-1}) at 80 °C and 60 %RH.

4.4. Conclusions

A series of STF polymers was successfully obtained to investigate the effects of trifluoromethyl groups on membrane properties. *Homo-*, *co-*, and *ter*-polymer with 3 different dichlorobenzotrifluoride monomers could not provide a good membrane due to low molecular weight. However, STF-BP copolymers consisting of synthesized dichloro-bis(trifluoromethyl)biphenyl provided flexible and transparent membranes. Approaching high IEC was very difficult due to the rigid backbone. The obtained STF-BP exhibited higher proton conductivity with higher water uptake than those of SBAF membranes. Particularly, under lower humidity, the proton conductivity of STF-BP membrane was significantly higher due to its gradual decrease compared to those of SBAF membranes with comparable viscoelastic stability. However, in tensile testing, the STF-BP membrane had significantly lower strain (< 20%). Although STF-BP membranes need to have improved elongation, which is difficult due to the rigid p-phenylene backbone, its proton conductivity, particularly under low humidity conditions, could be expected for enhanced properties of membranes.

References

[1] X. Chen, H. Lu, Q. Lin, X. Zhang, D. Chen, Y. Zheng, J. Membr. Sci., 2018, 549, 12-22

[2] S. Lee, J, Yuk, A. F. Nugraha, Y. Shul, S. Park, D. Shin and B. Bae, *Macromol. Mater. Eng.*, 2018, 303, 1700650

[3] L. Assumma, C. Iojoiu, R. Mercier, S. Lyonnard, H. D. Nguyen and E. Planes, *J. Polym. Sci., Part A: Polym. Chem.*, 2015, 53, 1941-1956

[4] H. Ono, J. Miyake, S. Shimada, M. Uchida, K. Miyatake, *J. Mater. Chem. A*, 2015, 3, 21779-21788.

Chapter 5. Conclusions and Future proposals

The widely useful proton exchange membranes are necessary to be further developed for application in PEMFCs. The excellent commercial perfluorosulfonic acid membranes (Nafion) have been used; however, inexpensive, and high-performance membranes have been required due to the drawback of Nafion membranes. Sulfonated aromatic polymeric materials have been promising as alternatives. Even though many researchers have suggested many enhanced new membranes, there is still a need to overcome several insufficient functions for application, such as high proton conductivity, reasonable durability to water-swelling, for example, mechanical stability under humid conditions, and compatibility with the catalyst layer. The purpose of this thesis was to investigate various chemically diverse structural effects on membranes properties.

In Chapter 2, two types of sulfonated terpolymers (SPA) containing perfluoroalkylene and alkylene group were successfully prepared, and the effects of both structures on the properties were investigated. According to the results, the excess ratio of alkylene groups compared with perfluoroalkylene groups causes lower solubility in polar organic solvents (like DMSO, DMAc and NMP), decreased proton conductivity, and well-developed hydrophobic morphology observed in TEM. Even though the OCV hold test of the SPA-cell revealed high oxidative durability of the SPA membrane with small loss in OCV value (the average decay of -120μV h^{-1}) for 1000 hours, the post-test durability analysis of the SPA membrane showed severe degradation in the alkylene group in the main chain. According to this result, alkylene groups might be inappropriate for long-term fuel cell operation conditions.

In Chapter 3, sulfonated aromatic polymers (SBAFs) containing sulfophenylene (SP) and hexafluoroisopropylidene biphenylene (BAF) groups were simply synthesized and compared with SPP-QP membranes to determine the effect of BAF groups on the membrane properties. As a result, introducing the BAF structure caused higher water uptake and proton conductivity but, interestingly, low mechanical elongation, even though the BAF (hexafluoroisopropylidene) group is less rigid than the quinquephenylene groups. However, slightly higher gas permeability and high oxidative stability of the SBAF membranes led to the result that the SBAF cell exhibited superior durability in the OCV hold test for 1000 hours, with very small decay in the OCV value (-40 μV h^{-1}), with slightly lower initial OCV of the SBAF cell (1.02 V) than the SPP-QP cell (1.05 V).

In Chapter 4, partially fluorinated sulfonated aromatic polymers (STF) were carefully designed and compared with SBAF membrane. In comparison with the SBAF membrane, the STF-BP membranes exhibited high proton conductivity, especially at less than 40% RH, and higher water uptake. However,

STF-BP cannot be prepared as high IEC (> 3.0 mequiv g^{-1}) membranes, and they exhibit very low elongation under humid conditions due to the very high rigidity of the membranes (associated with the p-phenylene component). In the future, it is necessary to find ways to overcome these drawbacks. As described in Figure 61, carefully optimized m- and p- mixed phenylenes could be expected to lead to improved elongation properties as modified SPP-QP membranes. The m-type of monomers will be prepared, and, at the same time, the preparation of m- and p-connected tetra-phenylene groups will be attempted.

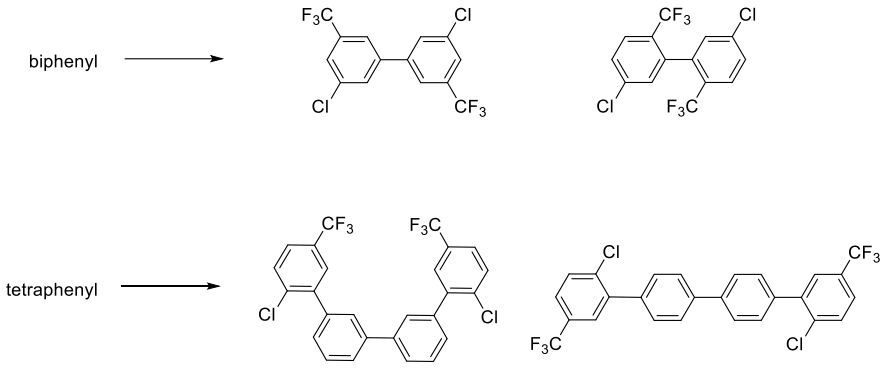

Figure 60. The chemical structure of expected partially fluorinated biphenyl and tetraphenyl monomers.

List of publications

1. Jinju Ahn, Kenji Miyatake, “Sulfonated Terpolymers Containing Alkylene and Perfluoroalkylene Groups: Effect of Aliphatic Groups on Membrane Properties and Interface with the Catalyst Layers”, *ACS. Appl. Energy Mater.*, **2018**, DOI: 10. 1021/acsaem.8b00684

2. Jinju Ahn, Ryo Simizu, Kenji Miyatake, “Sulfonated aromatic polymers containing hexafluoroisopropylidene groups: simple but effective structure for fuel cell membranes”, *J. Mater. Chem. A*, **2018**, DOI: 10.1039/c8ta09587f

Meeting abstracts

1. Jinju Ahn, Kenji Miyatake, “Synthesis and Properties of Sulfonated Terpolymers Containing Aliphatic and Perfluoroalkylalkyl Groups as Proton Exchange Membranes”, The 66th SPSJ Symposium on Macromolecules, 2017.09

2. Jinju Ahn, Kenji Miyatake, “Sulfonated Terpolymers as Proton Exchange Membranes for Fuel Cells: Effect of Aliphatic Groups”, 255th ACS National Meeting, 2018.03

3. Jinju Ahn, Kenji Miyatake “Synthesis and Characterization of Sulfonated Terpolymers Containing Perfluoroalkyl and Alkyl Groups for Application to PEMFC”, The 7th International Seminar on Green Energy Conversion, 2018.08

4. Jinju Ahn, Kenji Miyatake “Synthesis and Characterization of Sulfonated Terpolymers Containing Perfluoroalkyl and Alkyl Groups for Application to PEMFC”, The 8th International Fuel Cell Workshop 2018, 2018.08

5. Jinju Ahn, Kenji Miyatake “Synthesis and Properties of Sulfonated Poly(phenlyene)s Containing Hexafluoropropane Groups as Fuel Cell Membranes”, The 67th SPSJ Symposium on Macromolecules, 2018.09

Acknowledgements

This thesis is the summary of my research at the Clean Energy Research Center, Fuel Cell Nanomaterials Center and the Integrated Graduate School of Medicine, Engineering, and Agricultural Sciences at the University of Yamanashi, between 2016-2019.

I would like to express my deepest gratitude to my supervisor, Professor Kenji Miyatake of the University of Yamanashi. Having been under his tutelage for the entirety of my PhD, his consistent encouragement, invaluable advice, enlightening discussions, and positive influence have enabled me to avoid frustration.

I would like to express my gratitude to Professor Makoto Uchida of the University of Yamanashi for his warm encouragement, continuous consideration, and kindness.
I would like to express my gratitude to Professor Junji Inukai of the University of Yamanashi for his practical suggestions and warm encouragement.
I would like to express my gratitude to Associate Professor Junpei Miyake of the University of Yamanashi for his continuous support, beneficial instructions, invaluable help and advice.
I would like to express my gratitude to Associate Professor Shinji Nohara of the University of Yamanashi for his warm encouragement and kind consideration.
I would like to express my gratitude to Prof. Donald Alexander Tryk for his kindness, helpful English support, and useful advice.

I would like to express my gratitude to Professor Hiroyuki Uchida, Professor Akihiro Iiyama, and Professor Masahiro Watanabe of the University of Yamanashi for their support and encouragement.
I would like to express my gratitude to Professor Manuel Enuardo Brito, Professor Toshio Miyao, and Professor Katsuyoshi Kakinuma for their beneficial instructions and help.

I would like to express my gratitude to Dr. Byungchan Bae of the Korea Institute of Energy Research (KIER), a supervisor of my master's degree at the University of Science and Technology in Korea, for continuous invaluable support and advice. In particular, I am thankful for his encouragement to come study in Japan.

I would like to express my gratitude like to Dr. Young-Chul Park, former assistant professor at the University of Yamanashi, for his invaluable advice, support, and for leading me down the right path.

I would like to express my gratitude to Dr. Ryo Akiyama, Dr. Matsumoto Akinobu, and Dr. Naoki Yokota for technical support and practical discussions.

I would like to thank to all my membrane laboratory members, Mr. Ibuki Hosaka, Mr. Zhi Long, Mr. Keisuke Shiino, Mr. Takayuki Watanabe, Mr. Takatoshi Sawano, Ms. Mizuki Ozawa, Mr. Daniel Koronka, and Mr. Ryoji Nagasawa.

I would like to thank to Mr. Ryo Shimizu, Mr. Taro Kimura, and Mr. Toshiki Tanaka for technical support and useful discussions.

I would like to thank to all my former membrane laboratory members, Mr. Yao Jian Zhang, Mr. Ahmed M. A. Mahamoud, Mr. Hideaki Ono, and Ms. Manai Shimada for warm encouragement and help.

I would like to thank to all my research centre members, Mr. Hideaki Ohno, Mr. Shun Kobayashi, Mr. Ryo Kobayashi, Mr. Otsuji Kanji, and Ms. Rutsu Tamura for their kindness and help.

I would like to express my gratitude to Ms. Toshiko Gomyo for helping with TEM measurements and our informative discussions.

I would like to express my gratitude to Ms. Kaori Ichinose and the staff of the clean energy centre for their support and kindness.

Most importantly, I would like to thank to my father, mother, brother, brother's wife, and grandmother for their continuous encouragement and support.

I would like to thank to my friends in Japan for their kind help and for the unforgettable memories we shared. I'd also like to thank my friends in Korea for encouraging me and their helpful support.

March 2019

Jinju Ahn